Adiabatic shear banding and the micromechanics of plastic flow in metals

B. Gurrutxaga-Lerma

Trinity College Cambridge, Cambridge CB2 1TQ, UK and

*Department of Engineering, University of Cambridge, Trumpington St, Cambridge CB2 1PZ, UK**

This article studies the conditions that dislocation generation and motion must fulfil to promote the development of adiabatic shear bands in crystalline metals. First, we derive a stability criterion for the formation of shear bands, by linearising the conservation equations of thermo-plasticity. We then apply this criterion on the micromechanics-based Orowan equation for plastic flow, introducing a number of increasingly sophisticated constitutive assumptions on the model. It is found that there are two crucial promoters of shear band formation: the unfettered generation of dislocations that may be found in stage I plasticity; and the softening of the elastic constants with increasing temperature. In turn, we show that limiting the speed of dislocations tends to inhibit the formation of dislocations, even when the temperature dependence of the dislocation's drag is accounted for. This leads to the existence of an upper temperature limit above which shear band formation appears unlikely.

1. INTRODUCTION

Adiabatic shear bands consist of narrow regions of highly localised plastic deformation, which tend to arise in dynamic loading situations. Since they typically precede fracture, their formation becomes a critical mechanism governing the response of materials subjected to dynamic loading, as may be the case in chip formation during machining [1, 2], punching [3] and forging [4, 5], bird strikes on jet engines or airfoil leading edges [6], or in ballistic defeat of military armour [7], amongst other examples.

The conditions leading to the formation of a shear band have been studied since at least 1944, when Zener and Hollomon [8] associated shear band formation with the trade off between thermal softening and work hardening in the material. In subsequent decades, shear banding received ample attention, and it has usually been studied as an instability arising from the thermo-mechanical conservation equations applied across different lengthscales. Clifton [9, 10], Bai [11, 12], and Molinari [13, 14], amongst many others, derived instability criteria arising from studying the well-posedness of the thermo-plastic problem. Criteria of these kind have then been applied to a number of constitutive models, ranging from phenomenological [15] to plastic flow rules based on micromechanical considerations [16, 17], often aiming at predicting the width of the shear bands and the evolution of their properties [14, 18, 19]. As a result of these studies, Zener and Hollomon's original insight has been expanded, showing that shear banding is inhibited by inertial effects and promoted by thermal and strain softening [12, 19].

The conditions leading to the formation of shear bands vary depending on the loading conditions [19]. Generally, for moderate and high strain rates the primary mechanism for shear localisation is believed to be the thermo-plastic instability [20–22]. The latter may be brought about by a number of underlying physical processes, including the sudden release of dislocation pile-ups [23, 24], the heterogenous nucleation of dislocations [25], texture effects [26–28] and flow heterogeneities at stage II-III plasticity [14, 18, 29]. At lower strain rates,

* bg374@cam.ac.uk

shear bands may form via alternative softening mechanisms that do not necessarily fall within the remit of the thermo-plastic instability[30]. These include dynamic recrystallisation [30–32], damage[33], and even phase transformations [34].

The kinetics and kinematics of plastic flow therefore play a fundamental role in the formation of adiabatic shear bands: the availability of mechanisms able to produce sufficient plastic slip, sufficient local heating, and sufficient work hardening, is fundamentally limited by the loading conditions, which directly impart in the mechanics of dislocations, the discrete agents of plastic deformation[35]. If the timescales (and lengthscales) necessitated by the loading cannot be met by a specific dislocation mechanism (say, the thermal activation of dislocation motion[35]), alternative mechanisms (such as drag-dominated plasticity [28]) or radically different processes such as dynamic recrystallisation may dominate the formation of shear bands. The aim of this work is to study the way the micromechanics of plastic flow, understood as a dislocation mediated process, has in the formation of adiabatic shear bands, and the nature of dislocation-based physical mechanisms that dislocation-based physical models, such as constitutive laws employed at the macro scale or in crystal plasticity models, or models of discrete dislocation dynamics, would need to include to explain the onset of adiabatic shear bands, particularly at moderate to high strain rates. In this work, the micromechanics of plastic flow are modelled via the Orowan equation, which offers an exact average of the amount of plastic slip generated by a collective of dislocations in their generation and motion [35]. By introducing appropriate physical descriptions of both generation and motion processes at different strains, strain rates, and temperatures, this article offers a critical assessment of such processes, and the effect different physical mechanism have on the formation of shear bands.

This is because most studies of adiabatic shear localisation require making specific assumptions on the mathematical form of some constitutive law that describes the thermo-plastic behaviour of the material. The study of shear band formation therefore becomes a study of the well-posedness of flow rules against the thermal and mechanical conservation equations. Given the wide variety of plastic flow rules available, it is difficult to gain effective insights into the microscopic causes of the instability. The aim of this article is to investigate the physical conditions that contribute to the development of shear bands in the first place, by testing increasingly sophisticated flow rules based on Orowan's equation against an instability criterion. Specifically, we intend to examine the micromechanical conditions a system of dislocations needs to meet for shear bands to develop, as well as how constitutive models may be modified to reflect such conditions. As a result, the main concern of this article lies in the study of shear banding at moderate and high strain rates, where dislocation-based plasticity is expected to dominate the formation of shear bands [22].

In order to do that, this article is structured as follows: in section 2 we state the system of partial differential equations that will underpin the subsequent modelling of shear localisation. In section 3 we develop an instability criterion based on the ill-posedness of the problem; this will result in a comprehensive stability function that is explicitly dependent on the strain hardening (or softening), thermal softening (or hardening), and strain rate hardening irrespective of the form of the perturbation, and which may be applied to any constitutive model. Section 4 applies the resulting stability function to a series of increasingly comprehensive plastic flow rules modelled after the Orowan equation. This leads to the conclusion that it is the thermal softening of the elastic constants, rather than the thermal softening of the dislocation flow *per se*, that contributes most to the formation of shear instabilities in such models. Section 5 develops a more sophisticated micromechanical plastic flow model that encompasses a number of different microstructural effects, and is able to simulate plastic flow mechanisms across the strain rates. Finally, section 6 summarises the main findings of this article.

2. SHEARING MODEL

We shall first introduce the fundamental system of PDEs governing the thermo-plastic response of the material. The constitutive hypothesis of the model to be analysed are the following:

1. Compatibility of deformations

$$\dot{e}_{ij} = v_{i,j} \tag{1}$$

where $\dot{f} \equiv \frac{\partial f}{\partial t}$, e_{ij} is the strain tensor, and the $v_i = \dot{u}_i$ the displacement speed, with u_i the displacement vector.

2. Conservation of linear momentum

$$\rho \dot{v}_i = \sigma_{ij,j} \tag{2}$$

where ρ is the material's density, σ_{ij} is the Cauchy stress tensor.

3. The constitutive behaviour of the material is a function of strain, strain rate, and temperature:

$$\sigma_{ij} = f(e_{ij}, \dot{e}_{ij}, \theta) \tag{3}$$

where θ is the temperature.

4. Heat is produced by internal work of the material,

$$W = \int \sigma_{ij} e_{ij} \mathrm{d}V \tag{4}$$

a significant fraction of which is released as heat

$$Q = \beta W \tag{5}$$

where β is the Taylor-Quinney coefficient, $\beta \approx 0.8 - 0.9$ [36].

5. Heat diffuses according to Fourier's law, so that

$$\dot{Q} = \rho c_v \frac{\partial \theta}{\partial t} - \kappa \nabla^2 \theta \tag{6}$$

where c_v is the specific heat at constant deformation, and κ the thermal conductivity of the material.

Let the model be applied over a two-dimensional solid subjected to plane strain conditions, as depicted in fig.1. The only external applied load is a perfect shear stress, $\tau \equiv \sigma_{12}$. Let the loading conditions be translationally invariant in the x-direction; in that case τ is subjected to strain gradients only along the y direction. Accordingly, this pure shear stress state induces a pure shear strain $\gamma \equiv e_{12}$, and a corresponding shear strain rate

$$\dot{\gamma} \equiv \frac{\partial \gamma}{\partial t}$$

The conservation equations may then be reduced to the following:

$$\dot{\gamma} = \frac{\partial v}{\partial y} \tag{7}$$

$$\rho \dot{v} = \frac{\partial \tau}{\partial y} \tag{8}$$

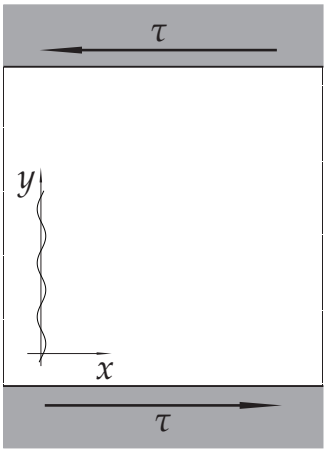

FIG. 1: Simplified shear system. Translational symmetry is assumed along the abscissae; the instability is assumed to take place along the ordinates.

$$\beta\tau\dot{\gamma} = \rho c_v \frac{\partial\theta}{\partial t} - \kappa\frac{\partial^2\theta}{\partial y^2} \tag{9}$$

subjected to the constitutive constraint

$$\tau = \tau(\gamma, \dot{\gamma}, \theta) \tag{10}$$

For simplicity, we shall assume that $\tau(\gamma, \dot{\gamma}, \theta)$, generally a non-linear function, is sufficiently smooth, continuously differentiable, and therefore satisfies the conditions of the implicit function theorem.

The state variables $\{\tau, \gamma, \dot{\gamma}, \theta\}$ are related to each other as follows

$$\frac{\partial\tau}{\partial y} = \left(\frac{\partial\tau}{\partial\gamma}\right)_{\dot{\gamma},\theta}\frac{\partial\gamma}{\partial y} + \left(\frac{\partial\tau}{\partial\dot{\gamma}}\right)_{\gamma,\theta}\frac{\partial\dot{\gamma}}{\partial y} + \left(\frac{\partial\tau}{\partial\theta}\right)_{\gamma,\dot{\gamma}}\frac{\partial\theta}{\partial y} \tag{11}$$

with

$$\left(\frac{\partial\tau}{\partial\gamma}\right)_{\dot{\gamma},\theta} \stackrel{\text{def}}{\equiv} A(y,t)$$

$$\left(\frac{\partial\tau}{\partial\dot{\gamma}}\right)_{\gamma,\theta} \stackrel{\text{def}}{\equiv} B(y,t)$$

$$\left(\frac{\partial\tau}{\partial\theta}\right)_{\gamma,\dot{\gamma}} \stackrel{\text{def}}{\equiv} C(y,t)$$

where A is the strain hardening function, B the strain rate hardening function, and C the thermal hardening function. Neither are assumed to be positive or negative (semi)definite a priori and, in fact, their nature in that respect remains material and loading dependent.

3. STABILITY ANALYSIS

Traditionally, shear bands have been analysed as arising from ill-posed conditions in the conservation equations that govern plastic flow [12, 37]. Therefore, in the following, by *stability* we refer to the well-posedness of the governing system of partial differential equations in the sense of Hadamard [38, 39], which concerns the case where the solution to the system of PDEs is ill-posed relative to perturbations of small wavelength — higher order perturbations would require more general spectral instability studies, and are omitted from this work.

3.1. Adiabatic case

If we examine the stability of the system for the adiabatic case, to wit, when the thermal conductivity $\kappa = 0$, we may rewrite the system as the following system of equations

$$\frac{\partial}{\partial t}\begin{bmatrix}\gamma\\ v\\ \theta\end{bmatrix} + \begin{bmatrix}0 & -1 & 0\\ -\frac{1}{\rho}A & 0 & -\frac{1}{\rho}C\\ 0 & -\frac{\beta\tau}{\rho c_v} & 0\end{bmatrix}\frac{\partial}{\partial y}\begin{bmatrix}\gamma\\ v\\ \theta\end{bmatrix} = 0 \tag{12}$$

[1] which may be condensed into the following first order PDE

$$\partial_t \mathbf{u} + \mathbf{M}(t, y, \mathbf{u})\partial_y \mathbf{u} = 0 \tag{13}$$

where $\mathbf{u} = (\gamma, v, \theta)^T$, and

$$\mathbf{M}(t, y, \mathbf{u}) \overset{\text{def}}{\equiv} \begin{bmatrix}0 & -1 & 0\\ -\frac{1}{\rho}A & 0 & -\frac{1}{\rho}C\\ 0 & -\frac{\beta\tau}{\rho c_v} & 0\end{bmatrix}$$

is a non-linear operator on the grounds that $\tau = \tau(\gamma, \dot{\gamma}, \theta)$; however, equation 13 is quasi-linear.

3.1.1. General case

Here we concern ourselves with the stability of eqn.13 subjected to Cauchy initial conditions, i.e.,

$$\mathbf{u}(y, 0) = \mathbf{u}_0(y) \tag{14}$$

This will represent an initial – even if sudden – value in strain, velocity or temperature field, which is entirely consistent with the expected loading a material may experience leading to the formation of a shear band.

Given the matrix $\mathbf{M}(t, y, \mathbf{u})$ above, unless the Jordan form of the matrix $\mathbf{M}(y, 0)$ is non-degenerate and real, the problem will be ill-posed in the sense of Hadamard [38] even if eqn.13 were to satisfy the Cauchy-Kowalevski theorem [40]. In this case, one finds that its normal Jordan form

$$\mathbf{J} = \begin{bmatrix}0 & 0 & 0\\ 0 & -\frac{1}{\rho}\sqrt{A_0\rho + \frac{\beta\tau_0}{c_v}C_0} & 0\\ 0 & 0 & \frac{1}{\rho}\sqrt{A_0\rho + \frac{\beta\tau_0}{c_v}C_0}\end{bmatrix},$$

with $A_0 = A(y, 0)$, $C_0 = C(y, 0)$, $\tau_0 = \tau(y, 0)$ is a non-degenerate real matrix if and only if

$$\left(\frac{\partial\tau}{\partial\gamma}\right)_0 + \frac{\beta}{\rho c_v}\tau_0\left(\frac{\partial\tau}{\partial\theta}\right)_0 > 0 \tag{15}$$

Recall that $A(y, 0)$ is a strain hardening parameter, and $C(y, 0)$ a thermal hardening parameter. For low strain rate behaviour, most metals are expected to display strong strain hardening (i.e., $A(y, 0) > 0$) and moderate thermal softening (i.e., $C(y, 0) < 0$), which entails there exists a relatively wide region of state variables for which the adiabatic problem may result in instability. The nature of these instabilities will depend on both the constitutive law (eqn.10) and the initial boundary conditions.

---

[1] The term $-\frac{1}{\rho}B\left(\frac{\partial\dot{\gamma}}{\partial v}\right)_{\gamma,\theta} = 0$

To illustrate the influence of the initial conditions, we may conceive of constitutive relation of the form

$$\tau = C\gamma^n\dot{\gamma}^m\theta^{-\nu}, \qquad n, m, \nu > 0, \tag{16}$$

which albeit empirical, contains all state variable dependences we may seek in the foregoing analysis. This constitutive law would represent *grosso modo* some material undergoing thermal softening, but strain and strain rate hardening, and should be valid for relatively low strain rates. For such constitutive law, stability requires that

$$\frac{n\rho c_v}{\nu\beta C} > \gamma^{n+1}(y,0)\dot{\gamma}^m(y,0)\theta^{-(\nu+1)}(y,0) \tag{17}$$

The inequality is guaranteed if:

1. $\theta(y,0) = 0$, which seems unlikely.
2. $\dot{\gamma}(y,0) = 0$, to wit, if the loading is quasi-static, which is consistent with the lack of shear bands in such loading regimes.
3. $\gamma(y,0) = 0$, that is, if no load is applied.

In practice, we may not be able to guarantee either condition outright. For instance, initial local strains may actually entail initial temperature increases due to the mesoscopic motion of dislocations, which brings about heat release. This ultimately means that at low strain rates *adiabatic* shear bands remain a distinct possibility.

Without assuming a form for the constitutive relation, if $A(y,0)$ and $C(y,0)$ are positive definite, i.e., if the material experiences strain hardening and thermal hardening at the same time, it also immediately follows that eqn.15 holds true for any initial condition. This is indicative that in the absence of heat transport, adiabatic shear bands ought not be able to form at high enough strain rates.

In addition, instabilities may arise if the material experiences strain softening (in which case $A(y,0)$ would be negative definite).

3.1.2. The role of temperature in the adiabatic case

Given that in the adiabatic case heat conduction is neglected, we may wonder whether, were the temperature state variable θ to be treated as a parameter instead (i.e., making $\theta =$ constant), we would still observe shear instabilities in the model. In that case, the system of equation reduces to

$$\frac{\partial}{\partial t}\begin{bmatrix} v \\ \gamma \end{bmatrix} + \begin{bmatrix} -\frac{1}{\rho}A & 0 \\ 0 & -1 \end{bmatrix}\frac{\partial}{\partial y}\begin{bmatrix} v \\ \gamma \end{bmatrix} = 0 \tag{18}$$

the stability of which is guaranteed given that $A \in \mathbb{R}, \quad \forall y, t \in \mathbb{R}$. This entails that shear bands can only form in the presence of a temperature field — the plastic problem on its own is well-posed.

3.2. The non-adiabatic case

In the event the material's thermal conductivity cannot be neglected, i.e, if $\kappa > 0$, the governing equations can't be reduced to a system of first order PDEs in the form of eqn.12, and the stability of the whole problem must be studied. Here, we follow Clifton [10] and Bai [11] in studying the stability of the eqn.12 by looking at the dispersion relation of the linearised system's solution.

By defining $\eta = \frac{\partial \theta}{\partial y}$, the system (eqns. 7, 8, and 9) may be expressed as

$$\begin{bmatrix} 1 & 0 & 0 & 0 \\ 0 & 1 & 0 & 0 \\ 0 & 0 & 1 & 0 \\ 0 & 0 & 0 & 0 \end{bmatrix} \frac{\partial}{\partial t} \begin{bmatrix} \gamma \\ v \\ \theta \\ \eta \end{bmatrix} + \begin{bmatrix} 0 & -1 & 0 & 0 \\ -\frac{1}{\rho}A & 0 & -\frac{1}{\rho}C & 0 \\ 0 & -\frac{\beta\tau}{\rho c_v} & 0 & -K \\ 0 & 0 & 1 & 0 \end{bmatrix} \frac{\partial}{\partial y} \begin{bmatrix} \gamma \\ v \\ \theta \\ \eta \end{bmatrix} = \begin{bmatrix} 0 \\ 0 \\ 0 \\ \eta \end{bmatrix}, \tag{19}$$

where $K = \kappa/(\rho c_v)$ is the thermal diffusivity.

The equation may be condensed into

$$\sum_{i=0}^{2} \mathbf{A}_i \partial_{x_i} \mathbf{u} = \mathbf{f} \tag{20}$$

where $\mathbf{x} = (t, y)^T$, $\mathbf{u} = (\gamma, v, \theta, \eta)^T$, $\mathbf{f} = (0, 0, 0, \eta)^T$, and

$$A_0 = \begin{bmatrix} 1 & 0 & 0 & 0 \\ 0 & 1 & 0 & 0 \\ 0 & 0 & 1 & 0 \\ 0 & 0 & 0 & 0 \end{bmatrix}, \quad A_1 = \begin{bmatrix} 0 & -1 & 0 & 0 \\ -\frac{1}{\rho}A & 0 & -\frac{1}{\rho}C & 0 \\ 0 & -\frac{\beta\tau}{\rho c_v} & 0 & -K \\ 0 & 0 & 1 & 0 \end{bmatrix}.$$

The system is strictly hyperbolic: since A_1 is nonsingular, we write,

$$|\alpha \mathbf{A}_1 - \lambda \mathbf{A}_0| = 0, \quad \forall \lambda \in \mathbb{R} \tag{21}$$

The roots α of this determinant are given by

$$\frac{\alpha\left(\alpha c_v \lambda^2 \rho^2 - A\alpha^3 c_v \rho\right)}{c_v \rho^2} = 0$$

which gives roots $\alpha_{1,2} = 0$, $\alpha_{3,4} = \pm\lambda\sqrt{\rho/A} \in \mathbb{R}$. Curiously, if the material experiences strain hardening, the system will remain hyperbolic, but if it experiences strain softening, the system will be of mixed hyperbolic-elliptic type. In either case, since some of these roots may be negative (λ is any one value in $\mathbb{R}$), the stability of the system is suspect.

a. Linearisation of the system. We now seek to linearise the system about a constant state $\mathbf{u}(y)$ such that it is compatible with the Cauchy boundary conditions $\mathbf{u}(y, 0) = \mathbf{u}_0(y)$. Given some equilibrium state $\mathbf{u}_0(y)$ such that $\mathbf{A}_1 \partial_y \mathbf{u}_0(y) = \mathbf{f}$, we therefore seek solutions of the form $\mathbf{u}(y, t) = \mathbf{u}_0(y) + \epsilon \boldsymbol{\upsilon}(y, t)$.[2] Accordingly, keeping only the terms of order ϵ, the linearised problem becomes $\mathbf{A}_0 \partial_t \boldsymbol{\upsilon} + \mathbf{A}_1^0(y) \partial_y \boldsymbol{\upsilon} = \mathbf{f}^0$, where $\mathbf{A}_1$ stands linearised as[3]

$$\mathbf{A}_1^0 = \begin{bmatrix} 0 & -1 & 0 & 0 \\ -\frac{1}{\rho}A_0(y) & 0 & -\frac{1}{\rho}C_0(y) & 0 \\ 0 & -\frac{\beta\tau_0(y)}{\rho c_v} & 0 & -K \\ 0 & 0 & 1 & 0 \end{bmatrix} \tag{24}$$

---

[2] That is, the state variables will be of the form,

$$\begin{aligned} \gamma(y,t) &= \gamma_0(y) + \epsilon g(y,t) \\ v(y,t) &= v_0(y) + \epsilon \mathrm{v}(y,t) \\ \theta(y,t) &= \theta_0(y) + \epsilon z(y,t) \\ \eta(y,t) &= \eta_0(y) + \epsilon e(y,t) \end{aligned} \tag{22}$$

[3] The linearised system will be

$$\begin{aligned} \partial_t g &= \partial_y \mathrm{v} \\ \partial_t \mathrm{v} &= \frac{A_0}{\rho}\partial_y g + \frac{C_0}{\rho}\partial_y z \\ \partial_t z &= \frac{\beta\tau_0}{\rho c_v}\partial_y \mathrm{v} - K\partial_y e \\ \partial_y z &= e \end{aligned} \tag{23}$$

We now want to study the normal modes of the linearised system. Specifically, we are concerned with the short wavelength disturbances about the equilibrium state $\mathbf{u}_0(y)$; this is because for short enough disturbances, $\mathbf{u}_0(y)$ will be approximately constant over the whole wavelength.

This entails seeking solutions to the linearised system of the form $\boldsymbol{\upsilon}(y,t) = \tilde{\boldsymbol{\upsilon}} e^{\sigma t + iky}$, where $\tilde{\boldsymbol{\upsilon}}$ are constants and $k \in \mathbb{R}$. Substituting, we obtain the following homogeneous system of equations

$$\begin{bmatrix} \sigma & -ik & 0 & 0 \\ -\frac{ik}{\rho}A_0 & \sigma & -\frac{ik}{\rho}C_0(y) & 0 \\ 0 & -\frac{\beta\tau_0 ik}{\rho c_v} & \sigma & -iKk \\ 0 & 0 & ik & -1 \end{bmatrix} \tilde{\boldsymbol{\upsilon}} = 0 \tag{25}$$

So we may only seek non-trivial solutions of the form $\boldsymbol{\upsilon}(y,t) = \tilde{\boldsymbol{\upsilon}} e^{\sigma t + iky}$ if the determinant of the matrix above vanishes, whereupon the dispersion relation of the solution $\boldsymbol{\upsilon}(y,t)$ is found to be:

$$c_v\rho^2\sigma^3 + c_v\rho^2 K k^2\sigma^2 + (A_0 c_v\rho + \beta C_0\tau_0)k^2\sigma - \ - A_0 c_v K\rho k^4 = 0 \tag{26}$$

The stability criterion is that $\mathrm{Re}[\sigma(k)] > 0$; otherwise, $\boldsymbol{\upsilon}(y,t)$ will tend to grow over time, perturbations will be magnified, and the problem will therefore be ill-posed.

As stated above, given that we have linearised the system, we can only properly study the stability of the system in a small neighbourhood about the equilibrium state, i.e., only for large values of k. Thus, albeit the dispersion relation $\sigma = \sigma(k)$ does have an explicit (albeit lengthy) solution via Cardano's formula, we can narrow our region of interest to asymptotic expansions of eqn.26 about $k \to \infty$, which render

$$-c_v\rho^2 K\sigma^2 + (A_0 c_v\rho + \beta C_0\tau_0)\sigma + A_0 c_v K\rho k^2 \approx 0 \tag{27}$$

So that to lowest order

$$\sigma = \frac{-(A_0 c_v\rho + \beta C_0\tau_0)}{2c_v K\rho^2}\left[1 \pm \sqrt{1 + \frac{4A_0 c_v^2 K^2\rho^3 k^2}{(A_0 c_v\rho + \beta C_0\tau_0)^2}}\right] \tag{28}$$

The solution is unstable for large k, but not in the sense of Hadamard. This general instability occurs when we have that

$$A_0 + \frac{\beta}{c_v\rho}C_0\tau_0 < 0, \tag{29}$$

that is, when

$$\frac{\partial\tau}{\partial\gamma} + \frac{\beta}{\rho c_v}\tau\frac{\partial\tau}{\partial\theta} < 0 \tag{30}$$

which is the same instability as the one obtained for the adiabatic case (eqn.15).

There exists a Hadamard instability, however, if

$$(A_0 c_v\rho + \beta C_0\tau_0)^2 \ll 4A_0 c_v^2 K^2\rho^3 k^2, \quad \text{for} \quad k \to \infty \tag{31}$$

This instability contains the inequality 30. Eqn.31 adds the additional condition that the instability will occur even if K is large. Therefore, in practice the Hadamard instability and the general spectral instability are the same.

The inequality 30 is contained in the one derived by Clifton [10] for the adiabatic case, but it does not display the effect of the strain rate hardening explicitly. This may be recovered however, if the system 19 is reformulated in terms of $\{\gamma, \dot{\gamma}, \theta\}$ as state variables. In that case, the dispersion relation becomes

$$c_v\rho^2\sigma^3 + \left(B_0 c_v k^2\rho + c_v k^2 K\rho^2\right)\sigma^2 + \left(A_0 c_v k^2\rho + B_0 c_v k^4 K\rho + \beta C_0 k^2\tau_0\right)\sigma + A_0 c_v k^4 K\rho = 0 \tag{32}$$

Proceeding as above, we find that to lowest order

$$\sigma = -\frac{\Gamma_3}{2\Gamma_1}\left[1 \pm \sqrt{1 - \frac{4\Gamma_1\Gamma_2}{\Gamma_3^2}}\right] \tag{33}$$

where

$$\Gamma_1 = B_0\rho c_v + K\rho^2 c_v, \quad \Gamma_2 = A_0 K\rho c_v$$

$$\Gamma_3 = A_0 c_v + B_0 c_v K\rho k^2 + \beta C_0\tau_0$$

Expanding eqn.34 in series about $k \to \infty$, one immediately finds that

$$\sigma = -\frac{A_0 + \frac{\beta}{c_v\rho}\tau_0 C_0}{2(B_0 + K\rho)} + \mathrm{O}\left[\frac{1}{k^2}\right] \tag{34}$$

The instability occurs if, in the $k \to \infty$ limit,

$$A_0 + \frac{\beta}{c_v\rho}\tau_0 C_0 < 0 \tag{35}$$

which is the already known eqn.30. The additional condition recovered here is that, for eqn.30 to be a source of instability

$$\frac{\partial\tau}{\partial\dot{\gamma}} + K\rho > 0 \tag{36}$$

Alternatively, if $A_0 + \frac{\beta}{c_v\rho}\tau_0 C_0 > 0$, we must have $\frac{\partial\tau}{\partial\dot{\gamma}} + K\rho < 0$; this would correspond to a material that displays a negative strain rate sensitivity, which has not been reported in practice (see [41]).

3.3. Stability function

In light of eqn.34, we may group together inequalities 30 and 36, to define the following stability function

$$V(t,y) = -\frac{\frac{\partial\tau}{\partial\gamma} + \frac{\beta}{\rho c_v}\tau\frac{\partial\tau}{\partial\theta}}{\frac{\partial\tau}{\partial\dot{\gamma}} + K\rho}, \tag{37}$$

so that the instability criterion is then be expressed as $V(t,y) > 0$.[4]

We note that because the PDE system was rewritten in terms of $\{\gamma, \dot{\gamma}, \theta\}$, we have achieved a stability criterion for the formation of shear bands that explicitly depends on inertial, thermal and strain effects in a single functional form that does not depend on the perturbation's wave number. Albeit is the combination of $\frac{\partial\tau}{\partial\gamma}$, $\frac{\partial\tau}{\partial\theta}$ and $\frac{\partial\tau}{\partial\dot{\gamma}}$ that determine the appearance of a shear instability, we may already notice that the latter is most likely if the material undergoes thermal softening (i.e., if $\frac{\partial\tau}{\partial\theta} < 0$), strain softening (i.e., if $\frac{\partial\tau}{\partial\gamma} < 0$). The former is a common occurrence at relatively high strain rates, whilst the strain softening is usual in stage I plasticity; inertial effects, in turn, appear to contribute to the stabilisation of the system.

---

[4] We note that the functional $\mathcal{V}[\tau] = \int V(t,y)\mathrm{d}t\mathrm{d}y$ is a Lyapunov functional candidate for the stability of the linearised system (similar remarks have been made by Markenscoff [42]), as it satisfies the central stability requirements that $\frac{\mathrm{d}\mathcal{V}}{\mathrm{d}t} \leq 0$, and that at $t = 0$ it is bounded by $|\tau(0,y)|^2$ [43].

4. STABILITY FUNCTION AND MICROMECHANICAL MODELS OF PLASTIC FLOW

The stability function V (eqn.37) has been derived under the assumption the material's behaviour may be expressed via a constitutive equation of the form $\tau = \tau(\gamma, \dot{\gamma}, \theta)$. The implied stability of any such constitutive law will depend on its constitutive assumptions, which in turn affect its appropriateness to model the loading regimes (i.e., temperature, strain rates, levels of strain,...) under which it may lead to instabilities and, as a result, the formation of shear bands.

In this section, we study the way the micromechanics of plastic flow — understood as the dislocation-based physical mechanisms that underpin microstructurally motivated constitutive models — influence the formation of adiabatic shear bands. This is achieved via Orowan's equation [44], which provides an average of the effect dislocation generation and motion have in the plastic strain (rate) of the material. By modifying the constitutive assumptions of Orowan's equation (in particular, the dislocation mobility and generation laws), we will produce a number of increasingly complex models of plastic flow to which the stability function V will be applied, to develop an understanding of the way different dislocation-based physical mechanisms may influence the formation of adiabatic shear bands.

Albeit it is not the aim of this work to produce perfect match to experiments, the models must fulfil a number of *desiderata* for them to be considered representative of empirical reality. Thus, there has to be a lower threshold strain rate, below which shear bands may not form [6]; there has to be an upper threshold temperature, above which shear bands may not generally form [45]. Shear banding must generally be easier to develop at higher strain rates [6, 37]. The constitutive models themselves ought to display strain rate sensitivity unless only low strain rates are being probed[46]; thermal softening ought to be expected at low strain rates[6, 35], and thermal hardening at high strain rates[47]. Yield drops, and subsequent strain hardening are sought at low strain rates [45].

In the following, we shall study the stability of a series of constitutive models that highlight specific aspects of the generation and motion of dislocations. As visual support, we shall plot the stability regions in conventional stress-strain curves. The focus of the work is in studying the physical conditions that contribute to the formation of shear bands, and not so much on providing quantitative matches to empirical data. For argument's sake, we shall build those stress-strain curves employing the usual elastic and micromechanical parameters of single-crystal aluminium, the values of which are detailed in the *Appendix*. The stress-strain curves usually extend from $\gamma = 0$ to $\gamma = 1$, simply to highlight the large levels of plastic deformation required for a shear band to develop.

4.1. Phenomenological power law.

In the event the constitutive relation takes the empirical form of eqn.16,

$$\tau = C\gamma^n \dot{\gamma}^m \theta^{-\nu}, \qquad n, m, \nu > 0$$

one can immediately check that the instability requirement for the Cauchy problem where

$$\tau(0, y) \equiv \tau_0(y) = C\gamma_0^n \dot{\gamma}_0^m \theta_0^{-\nu},$$

provides, via the V function, a lower bound for the strain rate

$$\dot{\gamma}_{\text{crit}} > \left(\frac{\rho c_v n}{C\beta\nu}\right)^{1/m} \gamma^{-\frac{n+1}{m}} \theta^{\frac{\nu+1}{m}} \tag{38}$$

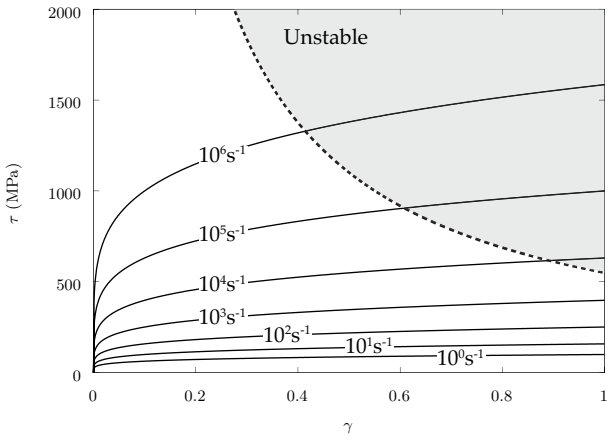

FIG. 2: Stress-strain curve and stability region for eqn.16. Note that the elastic response of the material has been neglected.

Figure 2 shows the resulting stress-strain curve at constant temperature and increasing strain rate, alongside the corresponding regions for which shear band formation is possible in this model. Although the figure does not intend to be representative of empirical reality but, rather, showcase the regimes of instability predicted by the theory, the material constants of aluminum have been used.

Eqn.38 displays a number of features that will be relevant to the foregoing analysis. First, as can be seen in fig.2, the formation of shear bands becomes increasingly likely with increasing strain rate. Second, the shear instability is all the likelier for thermal softening materials; in fact, eqn.38 highlights that the formation of a shear band is a trade-off between thermal softening and strain and strain rate hardening. Third, as has been remarked in the past (see for instance [6, 12]), we find that the strain rate hardening and the strain hardening tend to have a stabilising effect, and as was the case with adiabatic materials (see section 3 3.1), shear bands cannot form if the material displays thermal hardening i.e., a negative ν.

4.2. Orowan's equation

In the following, we will consider models of plastic flow based solely on physical considerations. These will be built solely on homogenised micromechanical considerations: dislocation speeds and dislocation densities will be treated explicitly to provide a better insight as to how these two parameters behave at the onset of a shear band.

Thus, given the unidimensional nature of the model, the following assumptions will be made

1. Plastic flow is governed by plastic slip alone; twinning, phase transformations, or any other source of permanent deformation are not accounted for.[5]

2. The material is assumed to be homogeneous and isotropic.

3. Plastic slip occurs around a single slip direction, the y-axis of the model.

4. The elastic response is neglected (i.e., all deformation is plastic).

[5] Albeit the focus of this work on shear banding warrants this assumption, it precludes the appearance of competing deformation mechanisms, such as dynamic recrystallisation at low rates or twinning that may at high enough rates overtake plastic slip and therefore inhibit the formation of shear bands.

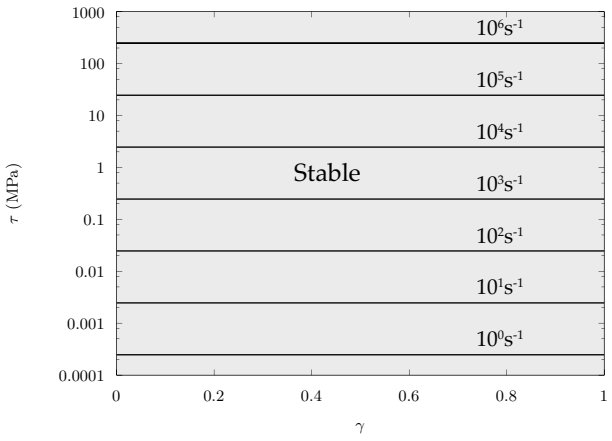

FIG. 3: Stress-strain curve and stability region for eqn.42. Note that the elastic response of the material has been neglected.

The (plastic) strain rate can then be modelled invoking Orowan's equation [44],

$$\dot{\gamma} = B\bar{v}\rho_m \tag{39}$$

where B is the magnitude of the Burgers vector, $\bar{v}$ the average dislocation glide speed, and ρ_m the mobile dislocation density. In order to ensure the general validity of Orowan's equation in the current setting, we assume that plastic flow is governed along a single slip direction that coincides with the y direction.

4.2.1. Drag-controlled plastic flow; moderate to high strain rates

In this section, we assume that plastic flow develops at strain rates high enough that dislocation glide is dominated by lattice drag. This is approximately accurate for most metals at strain rates above $\approx 10^3/s$[46]. In this event, the average dislocation speed will be directly proportional to the applied stress, via

$$\bar{v} = \frac{B\tau}{d} \tag{40}$$

where τ the applied stress and d the drag coefficient. The drag coefficient is usually directly proportional to the local temperature [35], via

$$d = \frac{d_0}{\theta_0}\theta \tag{41}$$

where d_0 is the drag coefficient at some reference temperature θ_0, and θ is the local temperature.

a. Unconstrained, drag-controlled plastic flow. We shall first assume that the mobile dislocation density remains constant and that the dislocations move in the drag-dominated regime i.e.,

$$\rho_m = \rho_{m_0} = \text{constant}, \quad \bar{v} = \frac{B\tau}{d} = \frac{B\theta_0}{d_0}\frac{\tau}{\theta}$$

so that the flow rule is

$$\dot{\gamma} = \frac{B^2\rho_{m_0}}{d_0}\frac{\tau}{\theta} \tag{42}$$

This describes a perfectly plastic material. That is, we are describing a plastic flow with no strain hardening and no strain rate effects. The stability function is

$$V = -\frac{\beta\Lambda}{\rho c_v}\frac{\dot{\gamma}^2}{1+\frac{K\rho}{\Lambda_1\theta}} < 0, \forall\theta > 0, \quad \Lambda_1 = \frac{d_0}{\rho_0 B\theta_0}$$

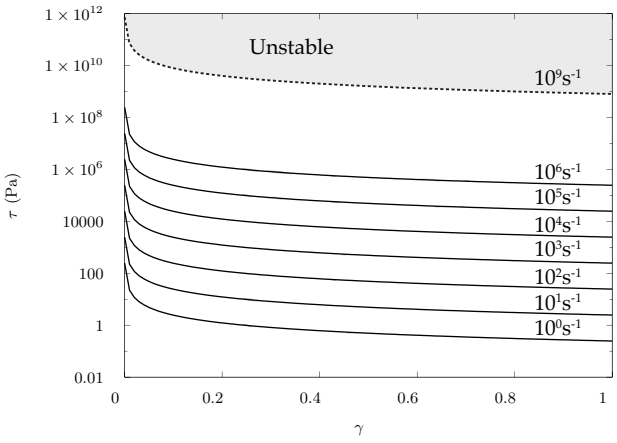

FIG. 4: Stress-strain curve and stability region for eqn.43. Note that the elastic response of the material has been neglected.

The model is therefore unconditionally stable, and will not leat to shear localisation. That is, for a plastic flow rule in which dislocations move unimpeded in a perfectly plastic regime, there is no shear banding. This is depicted in fig.3.

b. Free breeding, drag-controlled plastic flow. Amongst the many simplifications brought about by equation 42, the most immediate to consider is the assumption that the dislocation density is constant. This may be improved as originally done by Gilman [48], by assuming that each dislocation breeds a new dislocation upon having traveled some distance λ, whereby $\dot{\rho}_m = \rho_m \frac{\bar{v}}{\lambda}$. Since in Orowan's model $\rho_m \bar{v} = \frac{1}{B}\dot{\gamma}$, one finds that $\dot{\rho}_m = \frac{1}{B\lambda}\dot{\gamma}$, which may be integrated in time to get $\rho_m = \rho_{m_0} + \frac{1}{B\lambda}\gamma$, so that now the flow rule is

$$\dot{\gamma} = \left(\rho_{m_0} + \frac{1}{B\lambda}\gamma\right)\frac{B^2\theta_0}{d_0}\frac{\tau}{\theta} \tag{43}$$

In this case, strain softening is achieved via the dislocation density, which is posed to increase with strain; in turn, dislocation motion contributes to strain softening, and to thermal hardening. Moreover, the form of ρ_m is appropriate only for stage I plasticity, since dislocation generation is unconstrained in it. The stability function is

$$V = -\frac{B\lambda\dot{\gamma}\theta(\beta B\lambda\dot{\gamma} - \Lambda_2 c_v\rho)}{\Lambda_2 c_v\rho(B\lambda\rho_{m_0} + \gamma)(\Lambda_2 K\rho(B\lambda\rho_{m_0} + \gamma) + B\lambda\theta)}$$

where $\Lambda_2 = \frac{B^2\theta_0}{d_0}$. Assuming $\theta, \gamma > 0$, we find that the model is unstable either if $\dot{\gamma} < 0$, which is trivially discarded, or if

$$\dot{\gamma}_{\text{crit}} > \frac{B^2\theta_0 c_v\rho}{d_0\beta B\lambda} \tag{44}$$

For typical values in most metals, $\dot{\gamma}_{\text{crit}} \approx 10^9\text{s}^{-1}$. This is shown in fig.4, alongside the stress-strain curves prescribed by eqn.43. As can be seen, this model predicts a yield drop, strain softening and constant strain rate sensitivity; the former is empirically observed in many metals in stage I plasticity, but is subsequently followed by strain hardening as stage II overtakes plastic flow, which in this case is preempted by the constant increase in the mobile dislocation density. Although of limited practical use, the model highlights that materials undergoing strain softening may under some circumstances form shear bands. This possibility had already been noted in sections 3 3.3 and 4 4.1 when describing the V function and applying it to the power law. Here however we gain a physical insight as to what may promote such instability: the strain softening would be brought about by the unconstrained generation and motion of dislocations, and the competing hardening effect is due to the thermal

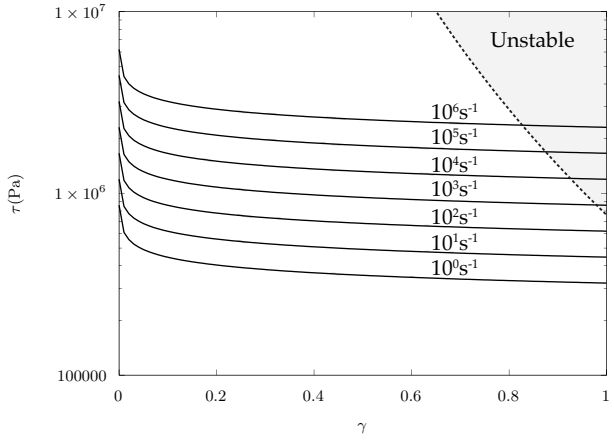

FIG. 5: Stress-strain curve and stability region for eqn.46. Note that the elastic response of the material has been neglected.

hardening implied by the lattice drag (see eqn.40). Clearly, this regime is only achievable at moderate and high strain rates (above $10^3 - 10^4 \mathrm{s}^{-1}$ for most FCC and HCP metals, perhaps higher for BCC metals[46, 47, 49]), where thermal hardening brought about by dislocation drag may dominate the plastic response. Still, the extremely high value predicted for $\dot{\gamma}_{\mathrm{crit}}$ in the model suggests that the instability will not take place if solely due to lattice drag, since at such high strain rates other effects, such as the relativistic motion of dislocations, will already dominate plastic flow[35, 50].

c. Velocity controlled plastic flow. Therefore, well before the $\dot{\gamma}_{\mathrm{crit}}$ in eqn.44 can be reached, the validity of the mobility law underlying $\bar{v}$ must be questioned. In particular, in the models above the mobility law was assumed to be governed by viscous drag forces, which remained in place irrespective of the stress level achieved. Albeit this is approximately true for dislocations moving in the *drag dominated* regime [35], dislocation velocity tends to saturate as the stress raises. This may be captured, albeit imperfectly, by considering a mobility law of the form [6, 48, 51]

$$\bar{v} = \frac{v_0 \theta_0}{\theta} \left(\frac{\tau}{\tau_0} \right)^m \tag{45}$$

which, albeit largely empirical, captures part of that saturation effect.

Therefore, let us assume that the flow rule is of the form

$$\dot{\gamma} = B \left(\rho_{m_0} + \frac{\gamma}{B\lambda} \right) \frac{v_0 \theta_0}{\theta} \left(\frac{\tau}{\tau_0} \right)^m \tag{46}$$

In this case, using V, we find that shear bands may form for strain rates above

$$\dot{\gamma}_{\mathrm{crit}} > \left(\frac{\gamma + B\lambda\rho_{m_0}}{\theta} \right)^{1-m} \frac{v_0 \theta_0}{\lambda} \left(\frac{c_v \rho}{\beta \tau_0} \right)^m$$

This prescribes a lower bound on the strain rate for the formation of shear bands that is now dependent on strain and temperature, and as is shown in fig.5, it gives rise to shear instabilities that are increasingly likely for higher strain rates.

There are a number of reasons why the material strain softens. On the one hand, the models employed so far assume a continuous increase in the mobile dislocation density; in order to maintain a constant $\dot{\gamma}$ with increasing γ, as the mobile dislocation density ρ_m increases the average dislocation speed $\bar{v}$ must decrease in equal proportion, which entails slowing dislocations and, consequently, a lower τ. Albeit the yield drop observed in many metals is associated with this effect [35], a flow model ought to allow for the more conventional strain

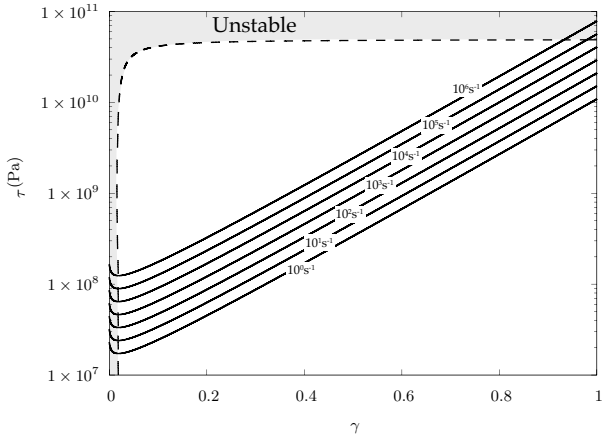

FIG. 6: Stress-strain curve and stability region for eqn.48. Note that the elastic response of the material has been neglected.

hardening, which is associated with dislocations hindering each other's motion via mutual interactions. On the other hand, the flow rules presume unimpeded dislocation motion, which does not hold in many metals, given the presence of obstacles in the form of phase boundaries, precipitates or other dislocations. Clearly both phenomena are intimately related: dislocation-obstacle interactions are bound to lower the mobile dislocation density.

d. Strain hardening plastic flow. Let us therefore consider a number of ways strain hardening may be introduced into Orowan's equation. On a first approach, we shall focus on the mobile dislocation density. As proposed by Gilman[48], if a fraction of dislocations are immobilised, then the mobile dislocation density ρ_m may be expressed as a fraction f of the total dislocation density, ρ_t:

$$\rho_m = f\rho_t$$

As a result of strain hardening, we introduce as an ansatz that the fraction f decreases over time in proportion to ρ_t, so that

$$\mathrm{d}f = -f\mathrm{d}\rho_t$$

The mobile dislocation density itself will still evolve in proportion to the strain, so that as before $\mathrm{d}\rho_t \propto \mathrm{d}\gamma$. In this case, we make $\mathrm{d}\rho_t = \Phi\mathrm{d}\gamma$, where Φ is an attrition coefficient accounting for mutual interactions, annihilations, dislocation-obstacle interactions and any other effect that may lower the fraction of mobile dislocations[48].

Thus, $\mathrm{d}f = -\Phi f\mathrm{d}\gamma$; integrating, we find $f = e^{-\Phi\gamma}$, and therefore

$$\rho_m = \left(\rho_{m_0} + \frac{\gamma}{B\lambda}\right) e^{-\Phi\gamma} \tag{47}$$

Therefore, this expression of ρ_m better accounts for stage I, II and III of plastic flow. Enabling strain hardening, one therefore gets a flow rule of the form

$$\dot{\gamma} = B\left(\rho_{m_0} + \frac{\gamma}{B\lambda}\right) e^{-\Phi\gamma} \frac{v_0\theta_0}{\theta} \left(\frac{\tau}{\tau_0}\right)^m \tag{48}$$

which using the V stability function leads to

$$\dot{\gamma}_{\mathrm{crit}} > B\frac{v_0\theta_0}{\lambda\theta}(\gamma + B\lambda\rho_{m_0})e^{-\Phi\gamma} \left(\frac{c_v\rho\theta(B\lambda(1-\rho_{m_0})-\gamma)}{B\beta\lambda\tau_0(B\lambda\rho_{m_0}+\gamma)}\right)^m$$

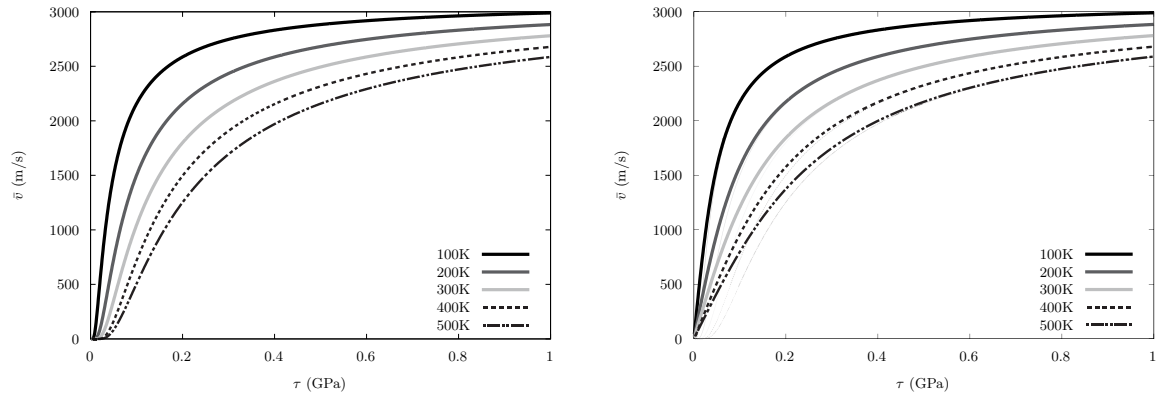

(a) Gilman's mobility model.

(b) Taylor's mobility model.

FIG. 7: Dislocation mobility models with $d_0 = 2 \cdot 10^{-5}$Pa·s, $c_t = 3100$m/s, $B = 2.85 \cdot 10^{-10}$m.

This leads to a lower and upper bound in strain for the formation of shear bands: the resulting stability region, shown in fig.6, shows that instabilities may happen either upon yielding, or at increasingly large strain rates. The lower, post-yield bound is associated with strain softening, which as was remarked in section 3 3.3 may be a source of shear instability, if present, since it entails negative $\frac{\partial \tau}{\partial \gamma}$ terms in the V function. The upper bound, in turn, is produced by the thermal softening of the material. One may also notice that the material described in fig.6 does now show a yield drop followed by strain hardening, but that its strain rate sensitivity remains constant for all strain rates. Thus, this model highlights that thermal hardening implied by lattice drag may facilitate shear localisation in stage I-II plasticity, thanks to the strain softening brought about by dislocation generation; and that in turn, at heating due to high strains dislocation glide may facilitate shear localisation under strain hardening implied by a saturating dislocation generation.

4.2.2. Relativistic motion of dislocations; high strain rates

A slightly more accurate description of the mobility of the dislocations themselves may be achieved by providing a mobility law that saturates as the dislocation approaches its limiting speed, generally accepted to be c_t, the shear wave speed [35]. This regime of dislocation motion, usually called *relativistic* [35], is expected to take place at strain rates above $\approx 10^6 \text{s}^{-1}$[52], and is brought about by the increasing dependence of the dislocation's own elastic self energy with its glide speed [35, 50]. A number of models of relativistic dislocation motion exist (see [50]). The most relevant implication that relativistic motion has with respect to adiabatic shear banding is that it imposes an upper limit to dislocation speed, thereby constraining plastic softening due to plastic slip. Here we therefore explore two different models of relativistic motion which capture this effect without adding increased complexities to the mathematical description of plastic flow.

a. Gilman's relativistic plastic flow. To begin with, we consider the mobility law originally proposed by Gilman as a phenomenological fit to experimental data (see [48]). It is of the form:

$$\bar{v} = c_t e^{-\frac{D\theta}{\tau}}, \quad D = \frac{c_t d_0}{2B\theta_0}$$

which is depicted in fig.7.a, and which renders the following flow rule

$$\dot{\gamma} = Bc_t \left(\rho_{m_0} + M\gamma\right) e^{-\Phi\gamma - \frac{D\theta}{\tau}} \tag{49}$$

where $M = 1/(B\lambda)$ when combined with the strain hardening proposed above.

The resulting stability function is

$$V = -\frac{D\dot{\gamma}\theta(\beta D(\gamma M + \rho_0) + c_v\rho(M(\gamma\Phi - 1) + \Phi\rho_0))}{c_v\rho(\gamma M + \rho_0)\left(D\theta + \dot{\gamma}K\rho\left(\Phi\gamma - \ln\left[\frac{Bc_t(\rho_0 + M\gamma)}{\dot{\gamma}}\right]\right)^2\right)}$$

Assuming that $\theta, \dot{\gamma} > 0$, both the numerator and the denominator are always positive. Thus, a model of plastic flow where dislocation velocity is constrained to be less than a limiting speed (in this case, the shear wave speed), appears to be unconditionally stable, and not lead to shear localisation. This highlights the strong reliance on the strain softening implied by unconstrained dislocation motion that the models presented in section 4 4.2 4.2.1 had: upon being constrained to an upper limit, as has been done here, dislocation motion appears to inhibit the production of adiabatic shear bands.

b. Taylor's relativistic plastic flow. Gilman's relativistic mobility is but one of a number of phenomenological fits to data that aim at describing the relativistic saturation of dislocation motion. In order to check that it is indeed the fact that dislocation motion is bound by an upper limit that inhibits the formation of shear bands. Alternatively, the saturation in the mobility may be achieved by requiring that

$$B\tau = \frac{d_0\theta/\theta_0}{1 - \bar{v}^2/c_t^2}\bar{v} \implies \bar{v} = \frac{d_0\theta c_t^2}{2\theta_0\tau B}\left(\sqrt{1 + \frac{4\tau^2B^2\theta_0^2}{d_0^2\theta^2c_t^2}} - 1\right)$$

This model, originally due to Taylor [48] was derived following arguments similar to the drag of electrons in a phonon gas.

Combined with the strain hardening dislocation density, one reaches a stability function of the form

$$V = -\frac{c_t^2d_0\dot{\gamma}\theta e^{\gamma\Phi}\left(c_v\rho\theta_0(M(\gamma\Phi - 1) + \Phi\rho_0)\left(B^2c_t^2(\gamma M + \rho_0)^2 + \dot{\gamma}^2e^{2\gamma\Phi}\right) + \beta c_t^2d_0\dot{\gamma}e^{\gamma\Phi}(\gamma M + \rho_0)^2\right)}{c_v\rho\theta_0\left(c_t^2d_0\theta(\gamma M + \rho_0)\left(B^2c_t^2(\gamma M + \rho_0)^2 + \dot{\gamma}^2e^{2\gamma\Phi}\right) + K\rho\theta_0e^{-\gamma\Phi}\left(\dot{\gamma}^2e^{2\gamma\Phi} - B^2c_t^2(\gamma M + \rho_0)^2\right)^2\right)}$$

Similarly to the prior case, there is no $\theta, \gamma, \dot{\gamma} > 0$ for which the stability function may become positive.

Thus, as with Gilman's mobility law, constraining the mobility of dislocations to an upper limiting speed with Taylor's mobility law appears to result in stable flow rules.

Taylor's mobility model has the virtue of, unlike Gilman's, immediately recovering the low speed viscous drag that is experimentally observed for overdamped motion of dislocations. As shown in fig.7, Gilman's mobility also entails a slight lag in reaching terminal speeds, but otherwise the differences between Gilman's and Taylor's model seem negligible, particularly in the asymptotic limit as $\bar{v} \to c_t$. Thus, it is not unexpected that both mobility models reach the same conclusion.

This is nonetheless a somewhat surprising conclusion, since it means that a relatively sophisticated micromechanical model, including physically meaningful phenomena such as strain hardening and limiting speeds for dislocations, fails to find a shear instability, whilst much more simple models find one.

Furthermore, in the asymptotic limit as $\bar{v} \to c_t$, the model becomes increasingly independent of temperature and very weakly dependent on strain and stress. There are two reasons for this: on the one hand, ρ_m tends to decrease with γ, due to the appearance of forest hardening effects; on the other hand, as $\bar{v}$ reaches values close to c_t, $\dot{\gamma}$ cannot increase any further as a result of an increase in τ. In this limit the model becomes insensitive to temperature, because crucially c_t has been assumed to be temperature independent. Added to this lack of thermal softening, the lack of plastic softening entails that the model is fully stable relative to the V function, and shear bands cannot form.

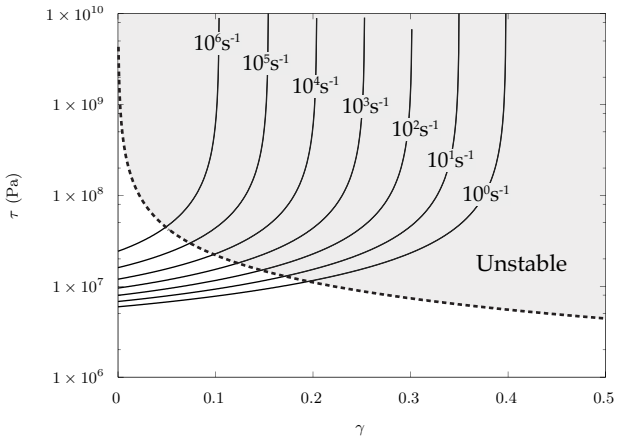

FIG. 8: Stress-strain curve and stability region for eqn.51.

c. Thermal softening of the elastic constants. One may therefore wish to consider a flow rule where the value of the limiting speed itself, c_t, is temperature dependent. In order to do so, we may asume as a first approach approximation that the material's density remains broadly unchanged with temperature, whilst the shear modulus tends to vanish as the material reaches its melting temperature θ_m. Thus, $\mu(\theta) = \mu_0(1-\theta/\theta_m)$, so that

$$c_t = c_{t_0}\sqrt{1-\frac{\theta}{\theta_m}} \tag{50}$$

Introducing the varying limiting speed on, say, eqn.49, we obtain the following flow rule

$$\dot{\gamma} = Bc_{t_0}\sqrt{1-\frac{\theta}{\theta_m}}\,(\rho_{m_0}+M\gamma)\,e^{-\frac{\gamma}{B\lambda}-\frac{D\theta}{\tau}} \tag{51}$$

The corresponding stability function is

$$V = -\frac{D\dot{\gamma}\theta\left(-2(\theta-\theta_m)(\beta D(\gamma M+\rho_0)+c_v\rho(M(\gamma\Phi-1)+\Phi\rho_0))\ln\left(\frac{Bc_{t_0}\sqrt{1-\frac{\theta}{\theta_m}}(\gamma M+\rho_0)}{\dot{\gamma}}\right)+\beta D(\gamma M+\rho_0)(2\gamma\Phi\theta-2\gamma\Phi\theta_m+\theta)+2c_v\gamma\Phi\rho(\theta-\theta_m)(M(\gamma\Phi-1)+\Phi\rho_0)\right)}{2c_v\rho(\theta-\theta_m)(\gamma M+\rho_0)\left(\gamma\Phi-\ln\left(\frac{Bc_{t_0}\sqrt{1-\frac{\theta}{\theta_m}}(\gamma M+\rho_0)}{\dot{\gamma}}\right)\right)\left(\dot{\gamma}K\rho\left(\ln\left(\frac{Bc_{t_0}\sqrt{1-\frac{\theta}{\theta_m}}(\gamma M+\rho_0)}{\dot{\gamma}}\right)-\gamma\Phi\right)^2+D\theta\right)}$$

This gives considerable scope for combinations of parameters leading to instabilities. Assuming $\theta, \gamma, \dot{\gamma} > 0$, we first note that in the denominator, the term

$$\gamma\Phi - \ln\left(\frac{Bc_{t_0}\sqrt{1-\frac{\theta}{\theta_m}}(\gamma M+\rho_0)}{\dot{\gamma}}\right),$$

is always negative for positive values of τ. Accordingly, we seek to make the numerator positive, which entails having an upper bound

$$\dot{\gamma}_{\text{crit}} < Bc_{t_0}\sqrt{1-\frac{\theta}{\theta_m}}(\gamma M+\rho_0)e^{\left(-\frac{\beta D(\gamma M+\rho_0)(2\gamma\Phi(\theta-\theta_M)+\theta)+2c_v\gamma\Phi\rho(\theta-\theta_M)(M(\gamma\Phi-1)+\Phi\rho_0)}{2(\theta-\theta_M)(\beta D(\gamma M+\rho_0)+c_v\rho(M(\gamma\Phi-1)+\Phi\rho_0))}\right)}$$

Figure 8 shows the corresponding stress-strain curve at constant temperature and for increasing strain rate. We observe a much wider region of instability, particularly with increasing strain rates; we also observe a noticeable strain rate sensitivity for the yield point at $\gamma = 0$, which had been missing in previous models. We note that these curves and regions of instability arise solely by assuming that the temperature affects (in practice, lowers) the limiting speed of the dislocations. When using the flow rule given in eqn. 49 the temperature dependence of c_t had been neglected, and as a result no shear instabilities were found. Thus, the crucial element in facilitating shear localisation at moderate and high strain rates appears to be the (local) thermal softening of the crystalline

lattice itself: albeit an increase in temperature will slow dislocations — which entails thermal hardening—, it will also soften the lattice, and in this case lead to a strong shear localisation principally due to the latter effect.

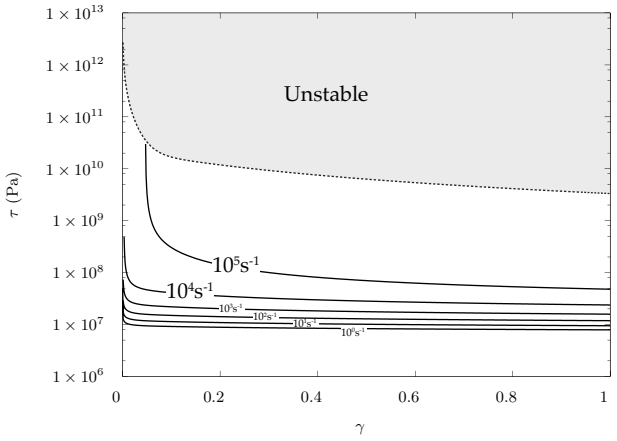

FIG. 9: Stress-strain curve and stability region for eqn.54. Here $a = 1.2$.

d. Further effects on the mobile dislocation density. The form of the mobile dislocation density employed so far,

$$\rho_m = (\rho_{m_0} + M\gamma)e^{-\Phi\gamma},$$

constitutes a broadly acceptable model of strain hardening effects. The first term $(\rho_{m_0} + M\gamma)$ would describe the evolution of the total dislocation density, and $e^{-\Phi\gamma}$ that of the fraction of mobile dislocations. Nevertheless, further refinements to this approach may extend the area of application of ρ_m to high strain rates; a number of such models are available, and have been employed successfully to model plastic flow in a number of metals (see for instance [53–55]).

In essence, these models rely on Hahn's [51] suggestion that the total dislocation density may better be represented by giving it a non-linear character

$$\rho_t = (\rho_0 + M\gamma^a) \tag{52}$$

via the exponent $a > 1$, followed by Yoshida's [53] proposal that the mobile dislocation density evolves from an initial value $f_0 = O(-6)$ to a final, non-zero saturated value $f_s = O(-3)$, whereby

$$f = f_0 + (f_s - f_0)(1 - e^{-\Phi\gamma}) \tag{53}$$

If we adopt this model rather than the simpler one employed before in, say, eqn.51, we define the following flow rule

$$\dot{\gamma} = Bc_{t_0}\sqrt{1 - \frac{\theta}{\theta_m}}\,(\rho_{m_0} + M\gamma^a)\left(f_0 + (f_s - f_0)(1 - e^{-\Phi\gamma})\right)e^{-\frac{D\theta}{\tau}} \tag{54}$$

We note that in general this model prescribes strain softening, since the existing population of mobile dislocation will tend to saturate to a certain non-zero fraction f_s.

Applying the V stability function to eqn.54, we find that the model entails a lower stability bound of

$$\dot{\gamma}_{\text{crit}} < Bc_{t_0}\sqrt{1 - \frac{\theta}{\theta_m}}\,(\rho_{m_0} + M\gamma^a)\left(f_s + (f_0 - f_s)e^{-\Phi\gamma}\right)e^{-\frac{\beta D\theta}{c_v\rho\left(\frac{2(f_0-f_s)\Phi}{f_0+f_s(e^{\Phi\gamma}-1)} + \frac{2\beta D}{c_v\rho} - \frac{2a\gamma^{a-1}M}{\rho_{m_0}+M\gamma^a}\right)(\theta-\theta_m)}}$$

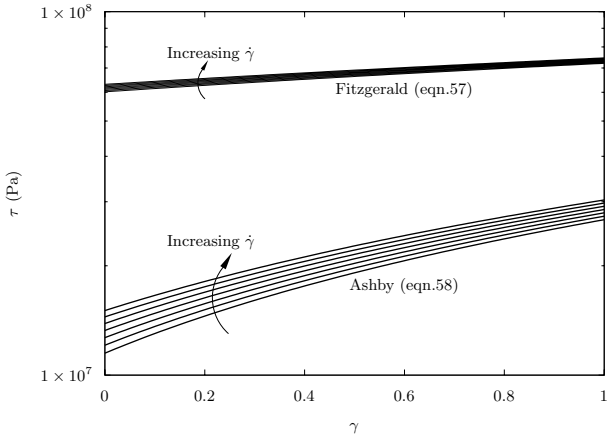

FIG. 10: Stress-strain curve for eqns.57 and 58. The models are stable throughout. Different values of M and ρ_0 have been chosen for eqn.57 (namely, $M = 5 \cdot 10^{15}\mathrm{m}^{-2}$ and $\rho_0 = 10^{15}\mathrm{m}^{-2}$) to avoid the overlap of both curves.

Both the resulting flow rules and region of instability are shown in fig.9. As remarked above, the model predicts strain softening, which may be more representative of empirical reality at higher strain rates, where these sorts of density evolution laws have been employed with greatest success [55, 56]. We also note that the stability of the model above is guaranteed if the elastic constants do not change with temperature; i..e, the flow rule

$$\dot{\gamma} = Bc_t \left(\rho_{m_0} + M\gamma^a\right)\left(f_0 + (f_s - f_0)(1 - e^{-\Phi\gamma})\right) e^{-\frac{D\theta}{\tau}}$$

can be proven stable relative to the V function. Hence, the crucial factor making this model unstable is, yet again, the softening of the elastic constants.

Thus, the physical cause of this instability appears to be related to the thermal softening of the elastic constants of the material; although this has been discussed in the past[57, 58], we note that in this model the result of increasing the temperature is not thermal softening, but hardening: *caeteris paribus*, increases in temperature in eqn.51 result in lower strain rates for the same applied stress.

A thermal hardening of the model is in principle consistent with dislocation theory, since in drag-controlled slip, dislocation drag is expected to increase in proportion to temperature. However, it should only occur for strain rates high enough that plasticity is in fact controlled by drag. For FCC and HCP metals, experimental evidence [47, 49] suggests that thermal hardening does in fact happen above $\approx 10^3 - 10^4\mathrm{s}^{-1}$ and beyond, and therefore the conclusions drawn above may apply for such materials.

4.2.3. Thermal activation of dislocation motion; low strain rates

a. Fitzgerald's and Ashby's thermally activated plastic flow. For BCC metals, where the Peierls barriers tend to be larger, plastic slip appears to be dominated over a much larger range by the thermally activated kink-pair mechanism to overcome the said barriers. Fitzgerald [59] has recently shown that the mobility of dislocations moving in both the thermal activation and the drag-controlled regimes may be correctly represented via a mobility law of the form

$$\bar{v} = C_1 e^{-\frac{8 + C_3\tau\left(1 - \ln\left[\frac{C_3}{16}\tau\right]\right)}{C_2\theta}} \tag{55}$$

On a first approach, we may simplify this into

$$\bar{v} = C_1 e^{-\frac{8+C_3\tau}{C_2\theta}} \tag{56}$$

This law is of the same form as the one proposed by Ashby and coworkers [45, 60] for plastic flows dominated by lattice resistance. Both models apply best at low strain rates, where the motion of dislocation is dominated by their ability to overcome, via thermal activation, lattice barriers[35, 45, 60].

If we employ these two models on equation 49, we reach the following flow rules

$$\dot{\gamma} = BC_1\left(\rho_{m_0} + M\gamma\right) e^{-\Phi\gamma - \frac{8+C_3\tau\left(1-\ln\left[\frac{C_3}{16}\tau\right]\right)}{C_2\theta}} \tag{57}$$

and

$$\dot{\gamma} = BC_1\left(\rho_{m_0} + M\gamma\right) e^{-\Phi\gamma - \frac{8+C_3\tau}{C_2\theta}} \tag{58}$$

The corresponding stability functions are

$$V = -\frac{C_2\dot{\gamma}\left(\beta(\gamma M+\rho_0)\left(\gamma\Phi-\ln\left(\frac{BC_1(\gamma M+\rho_0)}{\dot{\gamma}}\right)\right)\left(-C_2\theta\ln\left(\frac{BC_1(\gamma M+\rho_0)}{\dot{\gamma}}\right)+C_2\gamma\Phi\theta+8\right)+C_3c_v\rho\theta(M(\gamma\Phi-1)+\Phi\rho_0)W\left(\frac{-C_2\theta\ln\left(\frac{BC_1(\gamma M+\rho_0)}{\dot{\gamma}}\right)+C_2\gamma\Phi\theta+8}{16e}\right)\right)}{C_3c_v\rho(\gamma M+\rho_0)W\left(\frac{-C_2\theta\ln\left(\frac{BC_1(\gamma M+\rho_0)}{\dot{\gamma}}\right)+C_2\gamma\Phi\theta+8}{16e}\right)\left(C_3\dot{\gamma}K\rho W\left(\frac{-C_2\theta\ln\left(\frac{BC_1(\gamma M+\rho_0)}{\dot{\gamma}}\right)+C_2\gamma\Phi\theta+8}{16e}\right)+C_2\theta+C_3\dot{\gamma}K\rho\right)}$$

for eqn.57, and

$$V = -\frac{\dot{\gamma}\left(\frac{\beta C_2}{c_v\rho}\left(\gamma\Phi - \ln\left(\frac{BC_1(\gamma M+\rho_0)}{\dot{\gamma}}\right)\right)\left(8 + C_2\gamma\Phi\theta - C_2\theta\ln\left(\frac{BC_1(\gamma M+\rho_0)}{\dot{\gamma}}\right)\right) + C_2C_3\theta\left(\Phi - \frac{M}{\gamma M+\rho_0}\right)\right)}{C_3(C_2\theta + C_3\dot{\gamma}K\rho)}$$

for eqn.58. Here, $W(\cdot)$ is the Lambert Ω function (vid.[61]).

Given its greater mathematical simplicity, the Ashby model (eqn.58) appears to offer an immediate, analytical lower bound for the strain rate: $\dot{\gamma}_{\text{crit}} > BC_1(\gamma M + \rho_0)e^{\left(-\frac{\sqrt{\beta\left(16\beta(\gamma M+\rho_0)+C_2C_3c_v\rho\theta^2(-\gamma M\Phi+M-\Phi\rho_0)\right)}}{\beta C_2\theta\sqrt{\gamma M+\rho_0}}+\gamma\Phi+\frac{4}{C_2\theta}\right)}$ However, a careful examination of this bound shows that the term

$$\beta\left(16\beta(\gamma M + \rho_0) + C_2C_3c_v\rho\theta^2(-\gamma M\Phi + M - \Phi\rho_0)\right)$$

is generally negative because $\beta \ll C_2C_3\Phi\rho\theta^2/16$. This entails that the Ashby model is stable for the formation of shear bands.

Although it does not admit for an explicit lower bound, the Fitzgerald model can also be proven to be stable. The denominator of its stability V function is positive and cannot change sign, and the only terms that may cause the numerator to become negative cannot become negative. Indeed, the terms

$$\gamma\phi - \ln\left(\frac{BC_1(\rho_0 + M\gamma)}{\dot{\gamma}}\right) > 0 \forall \dot{\gamma}, \gamma > 0$$

because otherwise in eqn.57 $\dot{\gamma} < 0$, and for the same reason

$$-C_2\theta\ln\left(\frac{BC_1(\gamma M + \rho_0)}{\dot{\gamma}}\right) + C_2\gamma\Phi\theta + 8 > 0$$

Finally, $M(\gamma\Phi - 1) + \Phi\rho_0 > 0$ because $\Phi(\gamma M + \rho_0) \gg 1$. Hence, the Fitzgerald model is also stable for the formation of shear bands.[6]

---

[6] Frost and Ashby [45] propose a flow rule where the mobility rule given in eqn.56 is combined with a dislocation density evolves following Taylor's hardening, so that

$$\tau = \alpha\mu B\sqrt{\rho_m} \implies \rho_m = \left(\frac{\tau}{\alpha\mu B}\right)^2$$

Such model would be appropriate for modelling sigmoidal creep. Upon computing the stability function V, it can be shown that the model cannot become unstable either. A great deal of further refinements need be introduced to the expression of ρ_m to achieve an unstable model, usually aiming at modelling stage III-IV plasticity, where flow is dominated by avalanche-like effects. For instance, Molinari [14] achieved shear localisation by modelling stage III-IV plasticity via dislocation density.

Unlike Fitzgerald, Kocks and coworkers [46, 60] suggested that the mobility of dislocations the mobility of which is limited by lattice resistance (i.e., by the Peierls barrier, rather than by obstacles) ought to generally be of the form

$$\bar{v} = v_0 e^{-\frac{\Delta F}{k_B \theta}\left(1-\left(\frac{\tau}{\bar{\tau}}\right)^{3/4}\right)^{4/3}} \tag{59}$$

In that case, and allowing for strain hardening in the dislocation density, we reach a stability function of the form

$$V = -\frac{9\dot{\gamma}k_B\bar{\tau}\left(\beta\gamma\Phi\bar{\tau}(\gamma M+\rho_0)\left(1-\left(\frac{k_B\theta\left(\ln\left(\frac{Bv_0(\gamma M+\rho_0)}{\dot{\gamma}}\right)-\gamma\Phi\right)}{\Delta F}\right)^{3/4}\right)^{3/4}-\beta\bar{\tau}(\gamma M+\rho_0)\ln\left(\frac{Bv_0(\gamma M+\rho_0)}{\dot{\gamma}}\right)\left(1-\left(\frac{k_B\theta\left(\ln\left(\frac{Bv_0(\gamma M+\rho_0)}{\dot{\gamma}}\right)-\gamma\Phi\right)}{\Delta F}\right)^{3/4}\right)^{3/4}+c_v\rho\theta(\gamma M\Phi-M+\Phi\rho_0)\right)}{c_v\rho(\gamma M+\rho_0)\left(16\Delta F\dot{\gamma}K\rho\sqrt[4]{1-\left(\frac{k_B\theta\left(\ln\left(\frac{Bv_0(\gamma M+\rho_0)}{\dot{\gamma}}\right)-\gamma\Phi\right)}{\Delta F}\right)^{3/4}}\sqrt[4]{\frac{k_B\theta\left(\ln\left(\frac{Bv_0(\gamma M+\rho_0)}{\dot{\gamma}}\right)-\gamma\Phi\right)}{\Delta F}}+9k_B\bar{\tau}\theta\right)}$$

Again, it can be proven that neither the numerator nor the denominator may take non-positive values for $\theta, \gamma, \dot{\gamma} > 0$.

On a final note, we must remark that, in general, no model where the mobility of the dislocations takes an Arrhenius-like form, i.e., where

$$\bar{v} \propto e^{-\frac{E(\tau)}{k_B\theta}}$$

can develop adiabatic shear bands unless further effects such as strain softening contribute to the plastic flow. This is because if dislocation motion is governed by mechanisms described via transition state theory [7], the material will harden with increasing temperature, i.e., $\tau \propto \theta$; this effect will generally contribute to the stability of the V function, making the $\frac{\partial \tau}{\partial \theta}$ term more positive. As has been commented above, plastic flow is generally governed by Arrhenius forms at low strain rates and moderate stress levels, where no experimental evidence of adiabatic shear bands is generally found [6]. The transition between thermally activated and drag-controlled plastic flow is usually linked to an upshot in the strain rate sensitivity of the material; this transition typically occurs at $10^2 - 10^4 \mathrm{s}^{-1}$ for most cubic and HCP metals [41, 46]. Thus, we should only expect shear banding above such strain rates, unless strong plastic softening may otherwise be achieved. It must also be noticed that, as recently shown by Swinburne et al.[62], dislocation mobility may become temperature independent below certain levels of stress; under such conditions, shear localisation appears impossible too.

4.2.4. Final remarks.

This section has brought to light the way the kinetics of dislocation motion affect the formation of adiabatic shear bands. On the one hand, we have seen that the fundamental conditions leading to shear instabilities in micro-mechanical flow rules involve the ability of dislocations to glide to a good extent in the drag-controlled regime; i.e., adiabatic shear banding appears to be a phenomenon related to drag-controlled plasticity, which arises at moderate and high strain rates. Crucially, we have seen that the temperature dependence of drag-controlled (and relativistic) motion of dislocations entails thermal hardening, which inhibits shear band formation, unless the softening of the material's elastic constants is taken into account, which makes shear banding possible under certain conditions. In addition, strain softening due to sudden increases in ρ_m (or $\bar{v}$) appear to promote shear band formation. We also note the distinct effect the temperature and the strain rates have over the stability of the flow rules: whenever the instability is present, increasing the strain rate tends to make the model most likely to develop shear bands, as does increasing the temperature.

---

[7] As is the case of kink-pair mechanisms [59], or obstacle-dominated plasticity [45, 60].

On the other hand, we have also shown that low strain rate plastic flow, which is dependent on the thermal activation of dislocation motion, cannot produce shear bands: the Arrhenius-like temperature dependence of dislocation mobility appears incompatible with shear localisation if, as is to be expected, strain hardening is to take place. This entails that low strain rate plasticity requires large increases in ρ_m, and the concurrent local heating this would entail, if shear localisation is to take place. This only appears to be available at very large strain levels [14], or if additional mechanisms are modelled. In previous studies of the temperature rise due to a single moving dislocation (see [63]), the author found that the heating was mainly due to dissipative effects, but that one may only expect a sizeable local increase in the temperature when dislocations move in the so-called 'relativistic' (i.e., high speed) regime. Even then, the local temperature increase was found to be moderate, and not larger than $\approx 1 - 10$K, clearly insufficient on its own to justify a softening of the elastic constants. Thus, at low and moderate strain rates, the metal's ability to produce large, localised heating that would justify the softening of the elastic constants may only be achieved with dense distributions of fast moving dislocations. This may occur when a dense dislocation pile-up is suddenly released, as was suggested by Armstrong and coworkers [23]. This would invariably entail strain softening (ρ_m would suddenly increase), and local thermal softening, and therefore in light of the V function promote shear banding.

Thus, the models presented in this section suggest that unless large amounts of stored dislocation density can suddenly be released, at low strain rates dislocation plasticity on its own appears insufficient to produce the required plastic relaxation that will eventually lead to shear localisation. This would suggest that shear banding at low strain rates may only take place if additional effects other than those considered here dominate. In particular, the mechanism of dynamic recrystallisation by Rittel and coworkers [30–32], which is not accounted for in the current study, could be an alternative (and indeed, experimentally attested [31]) mechanism leading to shear banding. Other mechanisms, such as damage or phase transformations, may also play a role.

5. A MICROMECHANICAL PLASTIC FLOW MODEL

The models in section 4 for which the stability analysis has been performed tend to have a narrow region of physically meaningful application. Some, such as eqn.58, may only be employed to model creep and other extremely low strain rate phenomena; others, such as eqn.51, ought to be applicable in high strain rate deformation only. This is because in all cases the constitutive assumptions made to build the model tended to simplify the way dislocation density and dislocation speed may evolve for an envelope of variables $\{\gamma, \dot{\gamma}, \tau, \theta\}$.

In fact, one of the main criticisms of the stability analysis of flow models performed in section 4 is that the evolution of the density of mobile dislocations is not allowed to react to the enhanced or hindered mobility of the dislocations themselves, and remains largely independent from the loading state. Equally, even though section 4 has explored drag controlled, relativistic, and thermally activated dislocations, no unified flow rule that would encompass them all has been employed.

Here we aim to build a comprehensive constitutive relation that may be employed to study the leading causes of the shear instability, because it combines most of the physical mechanisms that have been discussed in section 4 as leading or inhibiting shear localisation across different strain rates.

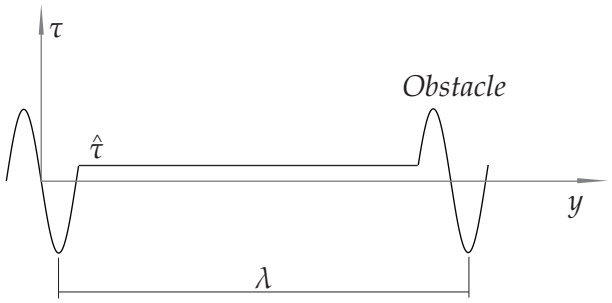

FIG. 11: Glide resistance profile. After [45].

5.1. Average dislocation speed

Here we follow Kocks et al. (1975) [60] in assuming that the average glide speed along the y-direction of a dislocation will be controlled by: (a) dislocation-obstacle interactions; (b) dislocation-background interactions; and (c) damping forces. Accordingly: (a) the dislocation spends a certain time $t_{\text{obstacle}} = f(\tau, \theta)$ trapped by each obstacle, which drops in value as temperature and stress levels increase; (b) the dislocation does not explicitly interact with other dislocations, but is subjected to a certain background stress $\tau(y)$; and (c) the dislocation moves between obstacles at the corresponding free glide speed $v(y)$, which is governed by viscous and radiative damping forces.

a. Dislocation-obstacle interactions. Obstacles represent impurities and precipitates. They are overcome by thermal activation, so that the time spent by the dislocation at the obstacle is of the form

$$t_{\text{obstacle}} = \frac{1}{\nu}\left(e^{\frac{\Delta F}{k_B \theta}} - 1\right) \tag{60}$$

The usual values of ν for a number of materials are listed in [45]. The form of ΔF, the free energy barrier, may change, but it is generally accepted to be of a form similar to the one that has been given in equation 56 when building the Fitzgerald-Ashby models. In particular, in invoking eqn.60, Frost and Ashby favour

$$\Delta F = \Delta F_0 \left(1 - \left(\frac{\tau}{\tau_0}\right)^a\right)^{1/a} \tag{61}$$

where $a < 1$. Clearly if $\tau > \tau_0$, the obstacle is overcome with no thermal activation.

b. Free glide between obstacles. The dislocation will be subjected to the applied stress τ, and the background stress $\hat{\tau}$, which represents lattice friction and barriers. Thus, the effective Peach-Koehler force $B(\tau - \hat{\tau})$ will balance the damping forces,

$$B(\tau - \hat{\tau}) = d_v v(y) \tag{62}$$

where d_v is the viscous drag coefficient. In order to account for radiative and viscous damping, and neglecting acceleration times, we employ Taylor's semi-phenomenological form for the drag coefficient (see [50]):

$$d_v = \frac{d}{1 - \frac{v(y)^2}{c_t^2}}, \tag{63}$$

where c_t is the transverse speed of sound, and d is the viscous damping coefficient. Combining eqn.62 and 63, one obtains an explicit expression for the glide speed

$$v(y) = \frac{dc_t^2}{2B(\tau - \hat{\tau})}\left[\sqrt{1 + \left(\frac{2B(\tau - \hat{\tau})}{dc_t}\right)^2} - 1\right] \tag{64}$$

Accordingly, if the average spacing between obstacles is some distance λ, the average glide time will be [60]

$$t_{\text{glide}} = \int_0^{\lambda} \left(\frac{dc_t^2}{2B\tau_{\text{eff}}(y)} \left[\sqrt{1 + \left(\frac{2B\tau_{\text{eff}}(y)}{dc_t} \right)^2} - 1 \right] \right)^{-1} \mathrm{d}y \tag{65}$$

where $\tau_{\text{eff}}(y) = \tau(y) - \hat{\tau}(y)$. For simplicity, we may assume that $\hat{\tau}(y) \equiv \hat{\tau}$ is approximately constant, as represented in fig.11. We may as well assume that the variations of $\tau(y)$ are small over the interval $[0, \lambda]$, so that $\tau_{\text{eff}} = \text{constant}$ and thus

$$t_{\text{glide}} \approx \frac{\lambda}{\frac{dc_t^2}{2B\tau_{\text{eff}}(y)} \left[\sqrt{1 + \left(\frac{2B\tau_{\text{eff}}(y)}{dc_t} \right)^2} - 1 \right]}$$

c. Temperature dependence of the glide speeds. A final note must be made regarding the temperature dependence of two parameters in this model. On the one hand, the viscous damping coefficient d, conveys both the fluttering and phonon and electron scattering effects. As stated in section 4, these effects entail a linear temperature dependence of d[64], whereby if d_0 is the value of d at some reference temperature θ_0, we have

$$d(\theta) = d_0 \frac{\theta}{\theta_0} \tag{66}$$

On the other hand, as done in section 4, the transverse speed of sound is $c_t = \sqrt{\mu/\rho}$ is temperature dependent because the material's density ρ and shear modulus μ are temperature dependent. In section 4 we have approximated this dependence by making $\mu = \mu_0(1 - \theta/\theta_m$. Although more sophisticated accounts may be invoked here (vid.[65]), we may improve this approximation via the correction proposed by Frost and Ashby [45],

$$\mu(\theta) = \mu_R \left[1 - \xi \frac{\theta}{\theta_m} \right] \tag{67}$$

where μ_R is some reference value of the shear modulus, $\xi = -\frac{\theta_m}{\mu_R} \frac{\mathrm{d}\mu}{\mathrm{d}\theta} \approx 0.5 - 0.9$, and θ_m the material's melting temperature. This model makes the shear modulus vanish at the melting point.

The density's temperature dependence is generally weaker, and will require invoking an equation of state such as the Mie-Grüneisen equation,

$$P = \frac{\rho c^2 \chi}{(1 - s\chi)^2} \left(1 - \frac{\Gamma_R}{2} \chi \right) + \Gamma_R E \tag{68}$$

where $\chi = 1 - \frac{\rho_R}{\rho}$, ρ_R the density at some reference temperature θ_R, c the bulk speed of sound at that temperature, P the material's pressure, Γ_R the Grüneisen parameter at the reference temperature,

$$E \approx \rho_R c_v (\theta - \theta_R)$$

the internal energy, and s the slope of the shock-Hugoniot (see [6]). As a first approach approximation, however, we shall assume that $\rho(\theta) \approx \rho_R$. Accordingly, we find

$$c_t(\theta) = c_t(\theta_R) \sqrt{1 - \frac{\theta}{\theta_m}} \tag{69}$$

with $c_t(\theta_R) = \sqrt{\mu_R/\rho_R}$. The average speed of the dislocation subjected to the state variables $\{\tau, \theta\}$ is then effective glide speed of the dislocation, which here is obtained as the average between the time spent held by an obstacle, and the time spent in free glide. If λ is the average distance between two obstacles, the effective speed will be

$$\bar{v} = \frac{\lambda}{t_{\text{obstacle}} + t_{\text{glide}}}, \tag{70}$$

Or, assuming $\tau_{\text{eff}} \approx$ constant over $[0, \lambda]$,

$$\bar{v} \approx \frac{\lambda}{\frac{1}{\nu}\left(e^{\frac{\Delta F}{k_B\theta}} - 1\right) + \frac{\lambda}{\frac{dc_t^2}{2B\tau_{\text{eff}}(y)}\left[\sqrt{1+\left(\frac{2B\tau_{\text{eff}}(y)}{dc_t}\right)^2}-1\right]}} \tag{71}$$

5.2. Evolution of the mobile dislocation density.

As laid out by Gilman [48], the variation in ρ_m over time is governed by three distinct processes: generation, annihilation, and immobilisation.

d. Dislocation generation Here, we shall allow for:

1. Homogeneous nucleation, only relevant at large strain rates that facilitate the true dislocation of the lattice which is usually modelled as [41]

$$\dot{\rho}_m|_{\text{hom}} = Ce^{-\frac{\Delta G_{\text{hom}}(\tau)}{k_B\theta}} \tag{72}$$

where C is a scaling factor, and ΔG_{hom} is the activation energy for homogeneous nucleation, which is stress dependent and here shall follow [66]

$$\Delta G_{\text{hom}} = \max\left\{2\pi R\frac{\mu B^2}{8\pi}\left[\frac{2-\nu}{1-\nu}\left(\ln\frac{8R}{a}\right)+\frac{1}{2}\right] + \gamma_{\text{SF}}A - BA\tau\right\} \tag{73}$$

where $A = \pi R^2$, γ_{SF} is the material's stacking fault energy, $a \approx 1.6B$ is the core radius, $R \approx 25\mathring{A}$ the newly created dislocation's loop radius.

2. Frank-Read source activity. Given a density of Frank-Read sources ρ_{FR} of average strength τ_{FR}, the average activation time may be estimated as [67]

$$t_{\text{FR}}(\tau,\theta) \approx \frac{\sqrt{2\beta d_0(\theta)\dot{\gamma}\mu^2\tau + \tau^2\tau_{\text{FR}}^2} - \tau\tau_{\text{FR}}}{2\dot{\gamma}\mu\tau} \tag{74}$$

so that

$$\dot{\rho}_m|_{\text{FR}} = \frac{\rho_{\text{FR}}}{t_{\text{FR}}(\tau,\theta)} \tag{75}$$

3. Cross-slip multiplication, which as poised by Gilman [48] is defined in terms of a fraction of the existing dislocation microstructure. If ρ_m is the pre-existing dislocation density, and dislocations moving with average speed $\bar{v}$ breed a new dislocation after some distance λ_{cs}, we find that

$$\dot{\rho}_m|_{\text{cs}} = \frac{1}{\lambda}\rho_m\bar{v} = \frac{1}{B\lambda}\dot{\gamma} \tag{76}$$

e. Annihilation. As their number grows, the probability of two unlike-signed dislocation segments annihilating each other increases. The probability that a dislocations encountering another ought to be proportional to ρ_m; given that two dislocations need to encounter for the annihilation to occur, the probability of the event will be proportional to ρ_m^2 [48], so that

$$\dot{\rho}_m|_{\text{annh}} = -\beta\rho_m^2 \tag{77}$$

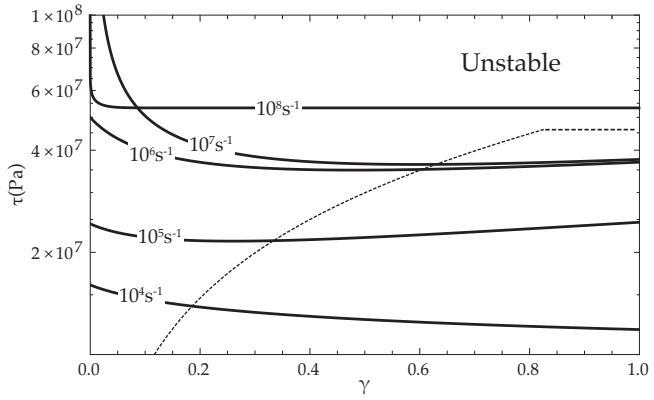

FIG. 12: Stress-strain curves for eqn.80 at 300K.

f. Immobilisation. This accounts for immobilisation of dislocations by obstacles or other dislocations. Given t_{obstacle} from eqn.60, we can define $f = 1/t_{\text{obstacle}}$ as the fraction of time a dislocation spends immobilised, whereupon

$$\dot{\rho}_m|_{\text{imm}} = -f\rho_m \tag{78}$$

As done in section 4 4.2, we now posit that f is of the form

$$f = e^{-\Phi\gamma}$$

where Φ is the attrition coefficient

These models effectively prescribe a variation of the dislocation density of the form

$$\dot{\rho}_m = \underbrace{Ce^{-\frac{\Delta G_{\text{hom}}(\tau)}{k_B\theta}} + \frac{\rho_{\text{FR}}}{t_{\text{FR}}} + M\dot{\gamma}}_{\text{Independent of } \rho_m} - f\rho_m - \beta\rho_m^2 \tag{79}$$

[8]

With these ingredients in mind, we are able to construct an approximative constitutive relation that reacts locally to changes in θ, γ, $\dot{\gamma}$ and τ:

$$\dot{\gamma} = \frac{B\lambda\rho_m(t,\tau,\theta)}{t_{\text{obstacle}} + t_{\text{glide}}} \tag{80}$$

5.3. Stability of the model and discussion

The flow rule given in eqn.80 includes refinements to all the models that have been presented in section 4. It is particularly suitable for studying high strain rate phenomena, because it accounts for both high rate generation mechanisms such as homogeneous nucleation and low strain rate ones such as cross glide breeding. Equally, it accounts for both low strain rate and high strain rate mobility phenomena.

The dislocation density is allowed to evolve in response to the kinetic state of the material; at constant strain rate, $\dot{\rho}_m$ in eqn.79 may be written as $\dot{\gamma}\partial\rho_m/\partial\gamma$, which is how we have estimated the stability region here.

[8] The equation can be rewritten as $\rho' = f(t) + a\rho - b\rho^2$; this can be turned into a linear ODE by letting $\rho = \frac{1}{b}\frac{u'}{u}$, whereupon we find

$$u''(t) - au'(t) - bf(t)u(t) = 0$$

which may be solved numerically more easily than the original equation.

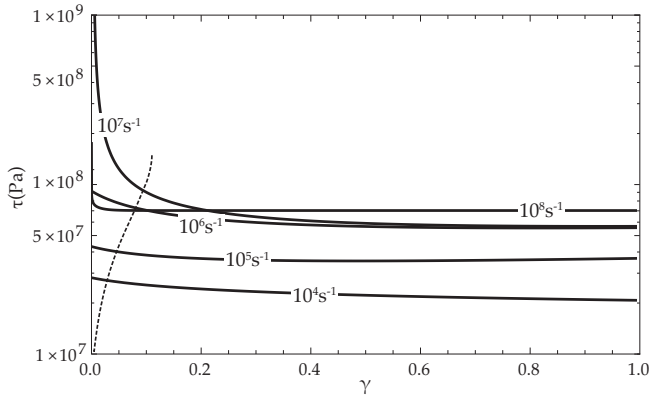

FIG. 13: Stress-strain curves for eqn.80 at 600K.

Figure 12 shows the regions of stability alongside the stress-strain curves at room temperature computed for this model, which largely corroborate the findings of section 4. For the parameters chosen for this model (see *Appendix*), we find that above a certain threshold strain rate (in between 10^7s^{-1} and 10^8s^{-1}), homogeneous nucleation takes over all other generation phenomena, which as can be seen in fig.12 entails a sudden yield drop followed by an almost perfectly plastic flow. The instability region widens for larger strains as one increases the strain rate; once homogeneous nucleation comes to dominate plastic flow, it appears the system becomes unconditionally unstable.

As can be see in fig.12, the model presented here invariably predicts a yield drop and strain softening; this clearly affects the instability region where shear bands may develop, that in this model is concentrated in the post-yield region, in a very similar way to how it was in eqn.48 (and fig.6). The role of the Ashby-like obstacle hopping term appears negligible above 10^4s^{-1}, and comes to dominate the response below that threshold, stabilising the model, which is why only strain rates above 10^4s^{-1} have been represented in fig.12. Temperature strongly affects the width of the instability region; upon being increased from 300K to 600K (i.e., from $\approx 1/3\theta_m$ to $\approx 2/3\theta_m$) as shown respectively in figs.12 and 13, we observe that the model becomes more stable. As we have commented in section 4, temperature appears to have a stabilising effect by means of increasing the dislocation drag; in section 4 this was balanced by the softening of the elastic constants with increasing temperature. Here, we observe that this stabilising effect tends to dominate as temperature is increased; in fact, as we discuss below, it seems that the effect leads to a critical temperature above which adiabatic shear banding does not seem possible. Otherwise, we must stress here that the main contributing factor to the instability of the model is the temperature dependence of the elastic constants, rather than the effect temperature has on the dislocation drag and on their generation.

A number of analytic asymptotic expressions may be computed to showcase the different stability limits brought about by the dominant role different generation and motion mechanisms acting at different strain rates and temperatures. For instance, for high strain rates (probably in excess of $\approx 10^7 - 10^8\text{s}^{-1}$[68]), generation is governed by homogeneous nucleation of dislocations that move at speeds approaching the limiting speed; neglecting any other generation mechanism, and assuming $\tau > \tau_{\text{hom}}$, we are in a regime where shear bands may form irrespective of the strain rate, but only so long as

$$\tau_{\text{crit}} \gtrsim -\frac{c_{t_0} D k_B}{2\Delta G_0(\xi\theta - \theta_m)} \left(3\theta^3 - 2\xi\theta^2\theta_m\right) \sqrt{1 - \xi\frac{\theta}{\theta_m}},$$

which suggests no shear bands may form unless $\theta < \frac{2}{3}\xi\theta_m$. Clearly, this limit is inherently dependent on the $\mu = \mu(\theta)$ relationship chosen here. Still, at very high strain rates this model prescribes a limiting temperature,

above which the material appears to favour plastic flow over shear banding which will be particularly appropriate for cubic metals, given that the constitutive assumptions of the model work best for them. Such upper limits in the temperature are commonly encountered in many metals [45].

The low strain rate regime, in turn, is governed by thermally activated dislocations hopping obstacles and lattice resistance; homogeneous nucleation is ruled out, and generation is governed by geometrical effects and low intensity sources. This regime is almost analogous to the Fitzgerald-Ashby models we have explored in section 4, and indeed, when testing the V model we find no instabilities leading to shear band formation. As previously stated, this regime is more appropriate to model creep and other extremely low strain rate phenomena.

The limitations of this model must also be highlighted, inasmuch as they may affect the physics underlying the formation of shear bands. On the one hand, the model clearly depends on a vast number of parameters, most of which are physically motivated but that can be estimated only over ranges of varied statistical significance. Although this reduces the ability to produce quantitative predictions with no a priori information on the exact values of those parameters, the model of shear band formation proposed here is able to make valuable qualitative predictions a priori, and may be applied to finely tuned models as well; the approach employed in building it is by no means unusual, and far more complex thermo-plastic models have been successfully employed to model low-to-high strain rate plastic phenomena [37, 55].

There are nonetheless a number of physically meaningful mechanisms that have been omitted from this discussion. In particular, heterogenous nucleation mechanisms have only been accounted for via Frank-Read sources, which at high strain rates appear to have no effect. Alternative heterogenous sources such as phase boundaries have not been accounted for in this model, despite the fact they may dominate the plastic response at high strain rates. Equally, if the generation rate is very high, the validity of the Orowan equation that has been used here can be brought into question, and could perhaps be substituted by the more accurate expression[69] $\dot{\gamma} = B\rho_m\bar{v} + B\bar{l}\dot{\rho}$, where $\bar{l}$ here is the average distance moved by a dislocation. We do not expect these effects to modify significantly the main conclusions of this work: on one hand many of these effects are implicitly accounted for in eqn.79; on the other, they will most likely promote enhanced strain softening, leading to at best a wider region of instability.

By encompassing a wide range of dislocation motion and dislocation generation mechanism that are active at different strain rates, strain levels, and temperatures, this model captures the relative importance of each at different strain rates, and the interplay between each other with respect to shear localisation. For instance, the model naturally accounts for the temperature dependence of the elastic constants at any strain rates; nevertheless, for thermally activated dislocations acting at low strain rates, this model shows that the impact this temperature dependence has on the formation of shear bands is negligible. This is not the case at high strain rates, where it was found to be the key destabilising physical mechanism. Equally, the effect of Frank-Read sources at high strain rates is seen to be negligible when compared to homogeneous nucleation when accounting for the expected strain softening due to such dislocation mechanisms, and therefore does not impact the formation of adiabatic shear bands.

6. CONCLUSIONS

This work has examined the micromechanical conditions that best explain the formation of adiabatic shear bands. A Hadamard stability criterion has been derived for general plastic flow rules. The stability criterion was able to capture inertial, strain hardening and thermal softening effects in a single functional form, irrespective

of the form of the perturbation, and it has been applied to a number of increasingly complex micromechanical models of plastic flow based on Orowan's equation. These models have focused on providing physical descriptions of both the kinetics of dislocation motion and dislocation generation, across a vast range of strain rates, temperatures, and levels of strain. This has enabled the study of the main destabilising physical mechanisms that may lead to the formation of adiabatic shear bands across the strain rates, highlighting: (a) the importance the kinetics of dislocation motion has in shear localisation; (b) the interplay between dislocation motion and dislocation generation that leads to shear banding; (c) upper and lower limits to the formation of shear bands, and how alternative mechanisms to dislocation-based plastic slip may be more likely responsible for shear localisation, particularly at low strain rates.

For low strain rates (below $\approx 10^3$s-1), we have shown that the thermal activation of motion of dislocations strongly inhibits the formation of shear bands, and that unless additional plastic softening may be achieved via strong mobile dislocation generation (as could be the case via the release of dislocation pile-ups), shear localisation may only be achieved via alternative mechanisms such as dynamic recrystallisation. Otherwise, this study shows that dislocation-based plasticity promotes shear banding when dislocations are moving in the drag-controlled and relativistic regimes, which dominate plastic flow at moderate and high strain rates.

The way drag-dominated plasticity promotes shear banding has been revealed to be complex. Lattice drag is directly proportional to temperature, and although it might seem that the latter's linear temperature dependence was responsible for leading to shear band formation, we have shown that it in fact has a stabilising effect in the formation of shear bands because it entails thermal hardening; it is due to strain softening or moderate strain hardening caused by the dislocation generation expected in stages I-II plasticity that shear localisation could develop. Crucially, simpler models lacking a limiting speed for dislocation motion have been found to be unstable; this is because of the unrestrained ability of dislocations to glide at any given speed , which promoted strain softening via plastic slip. At high enough strain rates –typically above 10^6s^{-1} [52]—, dislocation speed begins to saturate towards the shear wave speed, entering the regime of motion commonly called relativistic. When, under such loading conditions, dislocation motion was constrained to a given limiting speed, we found that shear band formation was inhibited, even if the dislocation drag was made to be temperature dependent. This was because relativistic dislocations were found to fundamentally constrain the material's strain softening and thermal hardening. However, when the model was modified to account for the lattice's own thermal softening via the temperature dependence of the material's own elastic constants, we found that shear banding became a distinct possibility again. Thus, at high strain rates we found that adiabatic shear banding would have been inhibited were it not for the local — and considerable — thermal softening of the material.

These results were further confirmed when building a constitutive model that accounted for all three dislocation motion regimes, alongside more physically accurate descriptions of thermal softening of the crystalline lattice, and a number of physically relevant dislocation generation mechanisms that may act across different strain rates were accounted for. This enabled us to explore the role Frank-Read sources, heterogeneous and homogeneous generation of dislocations may play in the formation of shear bands under high strain rates. We found that at moderate strain rates Frank-Read source generation may enter in competition with cross-slip multiplication and annihilations at low strain rates, confirming the expectation that shear localisation will be promoted by the lattice drag's thermal hardening and dislocation's motion plastic softening. At high enough strain rates, once homogeneous nucleation comes to dominate dislocation generation, plastic softening and localised heating meant that shear localisation became unconditional, up to a certain threshold value of temperature, above which shear banding was found to be impossible. This upper threshold was found to arise mainly

due to the thermal hardening implied by dislocation drag.

Thus, in this work we have found a number of physically-based mechanisms that, acting at different levels of strain, temperature, and strain rate, either contribute or inhibit shear localisation, and that often it is the interplay between these that makes shear band formation possible. The insights we have gained may be directly employed to assess the appropriateness of constitutive laws in the modelling of adiabatic shear banding phenomena, given that a number of usual assumptions, such as the thermal activation of dislocation motion, seem to be at odds with the possibility of shear localisation. Thus, this study enables modifications to existing constitutive models that would make them more physically relevant to shear banding, and the definition of new physically-based constitutive laws the ability of which to model shear localisation would be better understood. Furthermore, given that this study has helped shed light on the way dislocation generation mechanisms and dislocation kinetics influence shear localisation, the insights we have gained help in narrowing down the conditions that micromechanical simulations of discrete dislocation dynamics and phase field models must meet for adiabatic shear banding to occur. For instance, our results suggest that any constitutive or micromechanical model aiming at simulating shear band formation ought to allow for dislocations moving in the drag-controlled and relativistic regimes, account for the temperature dependence of both lattice drag and the elastic constants, and therefore promote situations where the strain rate is above $10^2 - 10^3 \mathrm{s}^{-1}$.

ACKNOWLEDGEMENTS

The author is grateful to the Master and Fellows of Trinity College Cambridge for munificently supporting him as a Title A Fellow.

APPENDIX

For the sake of argument, values referring to typical FCC materials such as Al have been used throughout. The parameters have been extracted from [45, 53, 70]. Unless otherwise stated, the following values have been employed: $\theta_0 = 300\mathrm{K}$, $\theta = 300\mathrm{K}$ (unless otherwise stated), $\theta_m = 933\mathrm{K}$, $\mu_0 = 25.3\mathrm{GPa}$, $\rho = \rho_R = 2700\mathrm{kg/m}^3$, $\beta = 0.9$, $c_v = 900\mathrm{J/(kgK)}$, $\kappa = 205\mathrm{W/(mK)}$, $B = 2.85\mathring{A}$, $\xi = 0.65$, $\Delta F = 0.5\mu B^3$, $\nu = 10^{-6}\mathrm{Hz}$, $d_0 = 2{\cdot}10^{-5}\mathrm{Pa{\cdot}s}$, $\Phi = 60$, $M = 10^{15}\mathrm{m}^{-2}$, $f_0 = 10^{-5}$,$f_s = 10^{-3}$, $\Delta G = g_0\mu B^3$, $\Gamma_R \approx 1.4$, $a = 2$, $\bar{\tau} = 10\mathrm{MPa}$,$\rho_0 = 10^{14}\mathrm{m}^{-2}$.

[1] R. Komanduri and B. F. Von Turkovich. New observations on the mechanism of chip formation when machining titanium alloys. *Wear*, 69(2):179–188, 1981.

[2] T. J. Burns and M. A. Davies. On repeated adiabatic shear band formation during high-speed machining. *International Journal of Plasticity*, 18(4):487–506, 2002.

[3] T. A. C. Stock and K. R. L. Thompson. Penetration of aluminum alloys by projectiles. *Metallurgical Transactions*, 1(1):219–224, 1970.

[4] S. L. Semiatin and G. D. Lahoti. Deformation and unstable flow in hot forging of Ti-6Ai-2Sn-4Zr-2Mo-0.1Si. *Metallurgical Transactions A*, 12(10):1705–1717, 1981.

[5] N.-K. Park, J.-T. Yeom, and Y.-S. Na. Characterization of deformation stability in hot forging of conventional ti–6al–4v using processing maps. *Journal of Materials Processing Technology*, 130:540–545, 2002.

[6] M. A. Meyers. *Dynamic behavior of materials*. John Wiley & Sons, New York, 1994.

[7] K. Maweja and W. Stumpf. The design of advanced performance high strength low-carbon martensitic armour steels: microstructural considerations. *Materials Science and Engineering: A*, 480(1):160–166, 2008.

[8] C. Zener and J. H. Hollomon. Effect of strain rate upon plastic flow of steel. *J. Appl. Phys.*, 15(1):22–32, 1944.

[9] R. J. Clifton. *On the analysis of elastic visco-plastic waves of finite uniaxial strain*, pages 73–116. Syracuse University Press, Syracuse, NY, 1970.

[10] RJ Clifton. Adiabatic shear banding. In *Material response to ultra high loading rates*, volume Report No. NMAB 356, 1980.

[11] Y. L. Bai. Thermo-plastic instability in simple shear. *Journal of the Mechanics and Physics of Solids*, 30(4):195–207, 1982.

[12] Y. Bai and B. Dodd. *Adiabatic Shear Localization*. Pergamon, 1992.

[13] C. Fressengeas and A. Molinari. Instability and localization of plastic flow at high strain rates. *Journal of the Mechanics and Physics of Solids*, 35(2):185–211, 1987.

[14] A. Molinari. Collective behavior and spacing of adiabatic shear bands. *Journal of the Mechanics and Physics of Solids*, 45(9):1551–1575, 1997.

[15] T. W. Wright and J. W. Walter. On stress collapse in adiabatic shear bands. *Journal of the Mechanics and Physics of Solids*, 35(6):701–720, 1987.

[16] R. W. Armstrong and F. J. Zerilli. Dislocation mechanics aspects of plastic instability and shear banding. *Mechanics of materials*, 17(2-3):319–327, 1994.

[17] J. R. Klepaczko and B. Rezaig. A numerical study of adiabatic shear banding in mild steel by dislocation mechanics based constitutive relations. *Mechanics of Materials*, 24(2):125–139, 1996.

[18] A.-S. Bonnet-Lebouvier, A. Molinari, and P. Lipinski. Analysis of the dynamic propagation of adiabatic shear bands. *International Journal of Solids and Structures*, 39(16):4249–4269, 2002.

[19] T. W. Wright. Theory of adiabatic shear bands. In Bradley Dodd, editor, *Adiabatic Shear Localization: Frontiers and Advances*, chapter 5, pages 215–246. Elsevier, London, 2nd edition, 2012.

[20] R. L. Woodward. Material failure at high strain rates. In J. A. Zukas, editor, *High-velocity impact dynamics*, pages 65–125, 1990.

[21] M. H. Miguélez, X. Soldani, and A. Molinari. Analysis of adiabatic shear banding in orthogonal cutting of ti alloy. *International Journal of Mechanical Sciences*, 75:212–222, 2013.

[22] A. Molinari, X. Soldani, and M. H. Miguélez. Adiabatic shear banding and scaling laws in chip formation with application to cutting of ti-6al-4v. *Journal of the Mechanics and Physics of Solids*, 61(11):2331–2359, 2013.

[23] R. W. Armstrong, C. S. Coffey, and W. L. Elban. Adiabatic heating at a dislocation pile-up avalanche. *Acta Metallurgica*, 30(12):2111–2116, 1982.

[24] R. W. Armstrong and W. L. Elban. Temperature rise at a dislocation pile-up breakthrough. *Materials Science and Engineering: A*, 122(2):L1–L3, 1989.

[25] J. J. Gilman. Micromechanics of shear banding. *Mechanics of Materials*, 17:83–96, 1994.

[26] M. Kuroda and V. Tvergaard. Effects of texture on shear band formation in plane strain tension/compression and bending. *International Journal of Plasticity*, 23(2):244–272, 2007.

[27] J. F. C. Lins, H. R. Z. Sandim, H.-J. Kestenbach, D. Raabe, and K. S. Vecchio. A microstructural investigation of adiabatic shear bands in an interstitial free steel. *Materials Science and Engineering: A*, 457(1):205–218, 2007.

[28] Z. Zhang, D. E. Eakins, and F. P. E. Dunne. On the formation of adiabatic shear bands in textured hcp polycrystals. *International Journal of Plasticity*, 79:196–216, 2016.

[29] A. Marchand and J. Duffy. An experimental study of the formation process of adiabatic shear bands in a structural steel. *Journal of the Mechanics and Physics of Solids*, 36(3):251–283, 1988.

[30] D. Rittel. A different viewpoint on adiabatic shear localization. *Journal of Physics D: Applied Physics*, 42(21):214009, 2009.

[31] D. Rittel, P. Landau, and A. Venkert. Dynamic recrystallization as a potential cause for adiabatic shear failure. *Physical review letters*, 101(16):165501, 2008.

[32] S. Osovski, D. Rittel, and A. Venkert. The respective influence of microstructural and thermal softening on adiabatic shear localization. *Mechanics of Materials*, 56:11–22, 2013.

[33] P. Longère, A. Dragon, H. Trumel, T. De Rességuier, X. Deprince, and E. Petitpas. Modelling adiabatic shear banding via damage mechanics approach. *Archives of Mechanics*, 55(1):3–38, 2003.

[34] S. P. Timothy. The structure of adiabatic shear bands in metals: a critical review. *Acta metallurgica*, 35(2):301–306, 1987.

[35] J. P. Hirth and J. Lothe. *Theory of dislocations*. Wiley, New York, 2nd edition, 1982.

[36] G. I. Taylor and H. Quinney. The plastic distortion of metals. *Phil. Trans. Roy. Soc. London A*, 230:323–362, 1932.

[37] T. W. Wright. *The Physics and Mathematics of Adiabatic Shear Bands*. Cambridge Univ. Press, Cambridge, UK, 2002.

[38] D. D. Joseph and J. C. Saut. Short-wave instabilities and ill-posed initial-value problems. *Theoretical and Computational Fluid Dynamics*, 1(4):191–227, 1990.

[39] G. Métivier. Remarks on the well-posedness of the nonlinear cauchy. *Geometric Analysis of PDE and Several Complex Variables: Dedicated to François Treves*, 368:337, 2005.

[40] L. C. Evans. *Partial Differential equations*, volume 19 of *Graduate Studies in Mathematics*. American Mathematical Soc., Providence, RI, 2nd edition, 2010.

[41] R. W. Armstrong, W. Arnold, and F. J. Zerilli. Dislocation mechanics of shock-induced plasticity. *Metallurgical and materials transactions A*, 38(11):2605–2610, 2007.

[42] X. Markenscoff. Hadamard instability analysis of "negative creep" in coupled chemo-thermo-mechanical systems. *Continuum Mech. Thermodyn.*, 28:351–359, 2016.

[43] V. I. Zubov. *Methods of A. M. Lyapunov and their application*. P. Noordhoff, Groningen, NL, 1964.

[44] E Orowan. Problems of plastic gliding. *Proceedings of the Physical Society*, 52(1):8, 1940.

[45] H. J. Frost and M. F. Ashby. *Deformation-Mechanism Maps: The Plasticity and creep of Metals and Ceramics*. Pergamon Press, Oxford, UK, 1982.

[46] G Regazzoni, UF Kocks, and P_S Follansbee. Dislocation kinetics at high strain rates. *Acta metallurgica*, 35(12):2865–2875, 1987.

[47] B. Gurrutxaga-Lerma, M. Shehadeh, D. S. Balint, D. Dini, L. Chen, and D. E. Eakins. The effect of temperature on the elastic precursor decay in shock loaded fcc aluminium and bcc iron. *International Journal of Plasticity*, 96:135–155, 2017.

[48] J. J. Gilman. *Micromechanics of flow in solids*. McGraw-Hill, New York, 1969.

[49] E. B. Zaretsky and G. I. Kanel. Effect of temperature, strain, and strain rate on the flow stress of aluminum under shock-wave compression. *Journal of Applied Physics*, 112(7):073504, 2012.

[50] B. Gurrutxaga-Lerma. The role of the mobility law of dislocations in the plastic response of shock loaded pure metals. *Modelling and Simulation in Materials Science and Engineering*, 24(6):065006, 2016.

[51] G. T. Hahn. A model for yielding with special reference to the yield-point phenomena of iron and related bcc metals. *Acta metallurgica*, 10(8):727–738, 1962.

[52] B. Gurrutxaga-Lerma, D. S. Balint, D. Dini, D. E. Eakins, and A. P. Sutton. A dynamic discrete dislocation plasticity method for the simulation of plastic relaxation under shock loading. *Proceedings of the Physical Society A*, 469:20130141, 2013.

[53] F. Yoshida. A constitutive model of cyclic plasticity. *International Journal of Plasticity*, 16(3):359–380, 2000.

[54] S. Avril, F. Pierron, M. A. Sutton, and J. Yan. Identification of elasto-visco-plastic parameters and characterization of Lüders behavior using digital image correlation and the virtual fields method. *Mechanics of Materials*, 40(9):729–742, 2008.

[55] J. L. Ding, J. R. Asay, and T. Ao. Modeling of the elastic precursor behavior and dynamic inelasticity of tantalum under ramp wave loading to 17 GPa. *Journal of Applied Physics*, 107(8):083508, 2010.

[56] J. L. Brown, C. S. Alexander, J. R. Asay, T. J. Vogler, D. H. Dolan, and J. L. Belof. Flow strength of tantalum under ramp compression to 250 GPa. *Journal of Applied Physics*, 115(4):043530, 2014.

[57] D. Bigoni and T. Hueckel. Uniqueness and localization–I. Associative and non-associative elastoplasticity. *International Journal of Solids and Structures*, 28(2):197–213, 1991.

[58] D. Bigoni and T. Hueckel. Uniqueness and localization–II. Coupled elastoplasticity. *International Journal of Solids and Structures*, 28(2):215–224, 1991.

[59] S. P. Fitzgerald. Kink pair production and dislocation motion. *Scientific Reports*, 6, 2016.

[60] U. F. Kocks, A. S. Argon, and M. F. Ashby. Thermodynamics and kinetics of slip. *Progress in Materials Science*, 19, 1975.

[61] R. M. Corless, G. H. Gonnet, D. E. G. Hare, D. J. Jeffrey, and D. E. Knuth. On the lambert W function. *Advances in Computational mathematics*, 5(1):329–359, 1996.

[62] TD Swinburne, SL Dudarev, and AP Sutton. Classical mobility of highly mobile crystal defects. *Physical review letters*, 113(21):215501, 2014.

[63] B. Gurrutxaga-Lerma. How strong is the temperature increase due to a moving dislocation? *International Journal of Solids and Structures*, 108:263–274, 2017.

[64] F. R. N. Nabarro. *Theory of crystal dislocations*. Clarendon Pr., Oxford, UK, 1967.

[65] DJ Steinberg, SG Cochran, and MW Guinan. A constitutive model for metals applicable at high-strain rate. *Journal of Applied Physics*, 51(3):1498–1504, 1980.

[66] S. Aubry, K. Kang, S. Ryu, and W. Cai. Energy barrier for homogeneous dislocation nucleation: Comparing atomistic and continuum models. *Scripta Materialia*, 64(11):1043–1046, 2011.

[67] B. Gurrutxaga-Lerma, D. S. Balint, D. Dini, D. E. Eakins, and A. P. Sutton. Attenuation of the dynamic yield point of shocked aluminum using elastodynamic simulations of dislocation dynamics. *Physical review letters*, 114(17):174301, 2015.

[68] B. Gurrutxaga-Lerma, D. S. Balint, D. Dini, and A. P. Sutton. The mechanisms governing the activation of dislocation sources in aluminum at different strain rates. *Journal of the Mechanics and Physics of Solids*, 84:273–292, 2015.

[69] MA Meyers, H Jarmakani, EM Bringa, and BA Remington. Dislocations in solids. *V*, 15:96, 2009.

[70] J. R. Davis, editor. *Aluminum and aluminum alloys*. ASM international, Materials Park, Ohio, 1993.